

**Synthesis of Novel MOFs, Characterization and Electrochemical  
Application for Water Splitting**



**Kainat Fatima**

**Reg. No. 331026**

A thesis submitted in partial fulfillment of requirements for the degree of

**Master of Science in Chemistry**

**Supervised by: Prof. M. Arfan**

Department of Chemistry


School of Natural Science


National University of Science and Technology


H-12, Islamabad, Pakistan 2022

## THESIS ACCEPTANCE CERTIFICATE

Certified that final copy of MS thesis written by **Kainat Fatima** (Registration No. **00000331026**), of **School of Natural Sciences** has been vetted by undersigned, found complete in all respects as per NUST statutes/regulations, is free of plagiarism, errors, and mistakes and is accepted as partial fulfillment for award of MS/M.Phil degree. It is further certified that necessary amendments as pointed out by GEC members and external examiner of the scholar have also been incorporated in the said thesis.

Signature:   
Name of Supervisor: Prof. Muhammad Arfan  
Date: 22/06/23


Signature (HoD):   
Date: 22/6/23

Signature (Dean/Principal):   
Date: 22/06/2023

**National University of Sciences & Technology****MS THESIS WORK**

We hereby recommend that the dissertation prepared under our supervision by: Kainat Fatima, Regn No. 00000331026 Titled: Synthesis of Novel MOFs, Characterization, and Electrochemical Application for Water Splitting be Accepted in partial fulfillment of the requirements for the award of **MS** degree.

**Examination Committee Members**

1. Name: PROF. HABIB NASIR Signature: 

2. Name: DR. MUHAMMAD ADIL MANSOOR Signature: 

Supervisor's Name PROF. MUHAMMAD ARFAN Signature: 

Co-Supervisor's Name PROF. MANZAR SOHAIL Signature: 

  
Head of Department

22/6/23  
Date

**COUNTERSIGNED**

Date: 22/06/2023

  
Dean/Principal

## **Acknowledgement**

First and foremost, I am thankful to Almighty Allah, who always blesses me and guides me to the right path and who gave me the strength to complete my degree. Blessings be upon Holy Prophet Muhammad ﷺ. I am also thankful to everyone who guided me through my journey.

I would like to thank to my Parents and siblings for their support and prayers without which my success would not be possible.

I express my gratitude from depth of heart to my supervisor **Prof. Muhammad Arfan** for his help and guidance during my thesis work. He guided me and solved all my problems during my MS. He was always available to guide and help his students. I am thankful to him.

I would like to express my deep appreciation to my co-supervisor **Prof. Manzar Sohail**, for their invaluable guidance and support throughout the entire process of researching and writing this thesis.

I am thankful to the GEC members **Prof. Habib Nasir** and **Dr. Muhammad Adil Mansoor** for their support and suggestions during my research. They not only supported me in the research but also guided each step of the research.

I would also like to acknowledge the co-operation of **Dr. Naseem** for CO<sub>2</sub> adsorption studies from **USPCASE, NUST Islamabad**.

Thanks to all my lab fellows, my class fellows, and my research fellows. Special thanks to my friends for their help during my research and provide a supportive and friendly behavior during the research.

Thanks to all my family for their prayers and support without which my work would not even be possible.

***Kainat Fatima***

## Abstract

Metal organic frameworks (MOF) is a porous material which is formed of organic ligand bonded with metal ion in an ordered network. Metal-organic frameworks, like zeolites, have porosities, but they may be made in an unlimited number of ways, with varying compositions and pore configurations. simple solvothermal synthesis was used to synthesize novel MOFs. The following techniques were used to characterize the synthesized MOFs: XRD, FT-IR, SEM, EDX, and TGA. The MOFs were put to the test for CO<sub>2</sub> adsorption and electrochemical water splitting. Zn-MOF demonstrated an overpotential of 340 mV with a current density of 230 mA/cm<sup>2</sup>, Y-MOF (1) demonstrated a lowest overpotential of 280 mV with a current density of 180 mA/cm<sup>2</sup>, and Y-MOF (2) demonstrated the highest overpotential of 420 mV. The Zn-MOF showed the lowest charge transfer resistance, which was about 2.418 ohm. To confirm the stability of catalysts, the MOFs were additionally chronopotentiometrically evaluated, they showed good stability for ten hours. The gas adsorption capability of Y-MOF (2) was moderate.

# Table of Contents

1. Chapter 1 .....	1
1.1 Introduction .....	1
1.2 Structural Properties of MOFs .....	2
1.3 Synthesis of MOFs .....	3
1.3.1 Conventional Method.....	3
1.3.2 Microwave Synthesis .....	4
1.3.3 Mechanochemical Method.....	5
1.3.4 Electrochemical Method .....	6
1.3.5 Sonochemical Method .....	6
1.3.6 Post Synthetic Modification Method. ....	7
1.4 Applications of MOFs .....	7
1.4.1 Drug Delivery Systems .....	7
1.4.2 Gas Separation .....	8
1.4.3 Heterogenous Catalysis.....	9
1.4.4 Sensors .....	9
1.4.5 Gas Storage .....	9
1.4.6 Water Splitting.....	10
1.5 Objectives.....	11
2. Chapter 2.....	11
2.1 Materials.....	11
2.1.1 Chemicals.....	11
2.1.2 Instruments and Equipment .....	11
2.2 Methodology .....	12

2.2.1	Synthesis of Schiff Bases.....	12
2.2.2	Schiff Bases Synthesized Using Salicylaldehyde and Three Different Amines.....	13
2.2.3	Synthesis of MOFs.....	15
2.2.4	Electrode Formation.....	16
2.2.5	Electrochemical Water Splitting.....	16
2.3	Characterization Techniques.....	17
2.3.1	X-ray Diffraction.....	17
2.3.2	Scanning Electron Microscopy.....	18
2.3.3	Energy Dispersive X-ray Spectroscopy.....	18
2.3.4	Fourier Transform Infrared Spectroscopy (FTIR).....	18
2.3.5	Electrochemical Studies.....	18
2.3.6	Calculation of Over Potential.....	19
3.	Chapter 3.....	20
3.1	Results and Discussion.....	20
3.1.1	Characterization of Schiff Base K-1.....	20
3.1.2	Characterization of Schiff base K-2.....	21
3.1.3	Characterization of Schiff Base K-3.....	22
3.1.4	Characterization of Zn-MOF.....	23
3.1.5	Characterization of Y-MOF (1).....	28
3.1.6	Characterization of Y-MOF (2).....	33
3.1.7	EDX of Y-MOF (2).....	36
3.2	Electrocatalytic Water Splitting.....	37
3.2.1	Linear Sweep Voltammetry of Synthesized MOFs.....	37
3.2.2	Electrochemical impedance Spectroscopy.....	38
3.2.3	Chronoamperometry.....	40

3.3	CO <sub>2</sub> Adsorption .....	41
4.	Work Summary .....	43
5.	Conclusion .....	43



## List of Figures

Figure 1: Synthetic Method of MOFs .....	3
Figure 2: Applications of MOFs .....	10
Figure 3: Pictorial Representation of Schiff Base Synthesis .....	12
Figure 4: Schematic Representation of MOF Synthesis .....	15
Figure 5: Electrode Formation and Electrochemical Setup .....	17
Figure 6: Reverse LSV of Zn-MOF for Calculating Overpotential.....	19
Figure 7 : FT-IR spectrum of Schiff Base (K-1).....	20
Figure 8: FT-IR spectrum of Schiff base (K-2) .....	21
Figure 9: FT-IR Spectrum of Schiff base (K-3).....	23
Figure 10: FTIR Spectrum of Zn-MOF/Schiff base (K-2) .....	24
Figure 11: XRD of as synthesized Zn-MOF.....	25
Figure 12: SEM Images of Zn-MOF at Different Resolutions .....	26
Figure 13: EDX of Zn-MOF .....	27
Figure 14: TGA of Zn-MOF .....	28
Figure 15: FT-IR of Y-MOF (1)/ Schiff base (K-1) .....	29
Figure 16: XRD of Y-MOF (1).....	30
Figure 17: SEM Images of Y-MOF (1) at Different Resolution .....	31
Figure 18: EDX of Y-MOF (1).....	32
Figure 19: TGA of Y-MOF (1).....	33
Figure 20: FT-IR of Y-MOF (2)/ Schiff base (K-3) .....	34
Figure 21: XRD of Y-MOF (2).....	35
Figure 22: SEM Images of Y-MOF (2) at Different Resolution .....	36
Figure 23: EDX of Y-MOF (2).....	37
Figure 24: Polarization Curves of all MOFs and Bare Ni-foam.....	38
Figure 25: EIS of Synthesized MOFs .....	39
Figure 26: Fitted circuit. ....	40
Figure 27: CP plot for MOFs .....	41
Figure 28: (a) Sorption Isotherm of Y-MOF (2) (b) Sorption Isotherm of Zn-MOF .....	42

## List of Tables

Table 1: CHN Analysis of Schiff Base (K-1) .....	20
Table 2: CHN Analysis of Schiff base (K-2).....	22
Table 3: CHN of Schiff base (K-3).....	23
Table 4: Overpotential Value of Synthesized MOFs .....	38
Table 5: Value of $R_{ct}$ of all MOFs .....	40
Table 6: Comparison of the results of OER of all MOFs .....	43

# 1. Chapter 1

## 1.1 Introduction

Porous compounds have exceptional characteristics like high surface area, surface chemistry (tunable) and steady pore size. These characteristics make these materials promising candidate for research. Numerous commercial applications, including molecular separations, gas storage, sensors, heterogeneous catalysis, and drug delivery, have shown significant promise for these porous materials. The properties of these materials can be further improved, and scientist of different fields are still working on it. Metal organic frameworks (MOF) is a porous material which is formed of organic ligand bonded with metal ion in an ordered network. Metal-organic frameworks, like zeolites, have porosities, but they may be made in an unlimited number of ways, with varying compositions and pore configurations. Starting in the 1960s, Tomic and others reported the existence of MOF-5 type structures. After the early 1990s, MOF research has grown significantly, particularly since Yaghi and his research team developed MOF-based porous materials<sup>1</sup>.

The term "organic SBU" (Secondary Building Units) refers to links made of organic materials as opposed to metal centers, which are known as inorganic SBU and act as "joints" in MOF structures. The three fundamental MOF components are its organic ligands, inorganic metal centers, and topographic anatomy. If MOFs were created by expanding zeolite topology, the porosity of their organic and inorganic structures would be higher than that of zeolites. The network's dimensions and the enlarged size of inorganic SBUs are the causes of the big pore size. Ordinarily, organic compounds are those that include one or more N or O donor atoms. As a bridge between metal ions, these molecules function as a conduit. Some of the commonest ligands are cyano groups, carboxylates, pyridyl and, polyamines, crown ethers, phosphonates, and especially ones produced from benzene, oxalic acid, and imidazole<sup>2</sup>.

It is possible to synthesize an infinite number of MOFs by combining different metal building blocks and organic linkers. The most notable distinction between MOFs and other porous materials is how highly adjustable they are. They can be tailored to have the desired structural, magnetic, catalytic, electrical, and optical properties. Numerous MOFs have been synthesized, for a variety of uses, like medication delivery, sensing, gas storage, catalysts, fuel cells, super capacitors, ion exchange, and gas separation.

To prepare Metal-Organic Frameworks (MOFs), inorganic and organic compounds with robust bonding (reticular synthesis). The adaptability of which can vary in components, form, size, and functionality prompted the reporting and examination of more than 20,000 distinct MOFs within the last ten years. Thousands of compounds have been prepared thanks to the versatility of metal SBUs and organic linkers and studied annually.

## **1.2 Structural Properties of MOFs**

There are two types of components present in the structure of MOFs: secondary building units (metal ions) and organic linker<sup>3</sup>. These simple geometric forms depict the inorganic clusters or coordination spheres that are linked by the (typically linear) biological components to form the product structure<sup>4</sup>.

Secondary building units (SBUs) that build the network symmetry are formed by the topology of MOFs, which is related to both the coordination environment preferred by the metal ion and the geometry of the organic ligands. MOFs can be modified to suit certain purposes by changing the metals, ligands, and linkers that make them up. The ability to alter the pore size and chemical environment to obtain features is made possible by the existence of both inorganic and organic components. This distinguishes MOFs from zeolites, which are both crystalline and microporous but are entirely inorganic and have little ability to be synthesized. Metal nodes and organic linkers self-assemble to form rigid pores that are extremely durable and do not collapse when the solvent or other "guest" molecules that were filling the pores during synthesis are removed. This process generates permanent porosity<sup>5</sup>.

The organic ligands used to make MOFs have several binding sites for constructing the framework. By using adaptable stiff ligands during synthesis, it is possible to regulate the structural variety of MOFs. A thorough analysis of organic linkers is helpful for determining the fate of MOFs because the applications and utility of MOFs are dependent on the choice of organic ligands. The choice of organic ligands, including their flexibility or rigidity, has a significant impact on how networks form<sup>6</sup>. Numerous issues, such as unusual geometry, are caused by the flexible ligand's various conformations. In creating a sturdy structure, the rigid ligand was helpful. To prevent the electrons participating in coordination from freely rotating, rigid ligands like 4, 4'-bipyridine can be utilized as the network's supporting structure. Stiff ligands are used to build frames to prevent structural issues with the network. The construction

of frameworks uses ligands with multiple coordination centers; heteroatoms like N and O serve as the active sites for ligand attachment to metals<sup>7</sup>.

### 1.3 Synthesis of MOFs

By using a process known as "modular synthesis," MOFs are typically created by slowly growing crystals from a heated solution using a nucleation and growth mechanism to create porous structures<sup>4</sup>. There are several ways to make MOFs, including conventional synthesis (solvothermal included), microwave, electrochemical, mechanochemical, and sonochemical<sup>3</sup>.

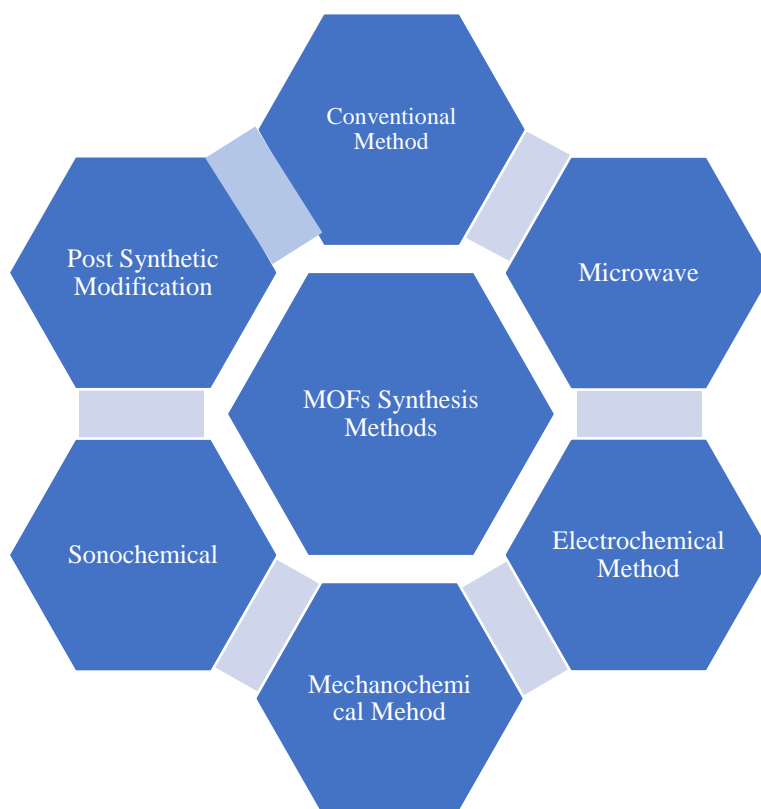


*Figure 1: Synthetic Method of MOFs*

#### 1.3.1 Conventional Method

The two subclasses of conventional synthesis are solvothermal and non-solvothermal. The term "solvothermal" is more inclusive than the phrase "hydrothermal," with water acting as the solvent. Non-solvothermal synthesis takes place in open flasks at atmospheric pressure below the

solvent boiling point, whereas solvothermal synthesis is done in specialized closed chemical reactors under elevated pressure brought on by the solvent vapor or else generated via a pump. Non-solvothermal synthesis can be conducted both at room temperature and while being heated; it does not require sophisticated equipment. A typical plan for this type of synthesis calls for selecting the salt (metal source), organic linker, solvent, and adjusting pH and temperature to produce the target MOF with the highest yield possible. The reagent concentrations should be chosen accordingly that the nucleation requirements are met for a precipitate to develop. This is usually facilitated by increasing the temperature, which causes the solvent to evaporate. Additionally, the solution can be slowly cooled, layers of solvent can form, or one of the reactants can diffuse slowly to create a concentration gradient. Solvothermal synthesis enables increased product yields and better crystallinity. Due to the increased pressure, the solvent can be heated to its boiling point (at a pressure of 1 atm), which enhances the solubility of the reactive salts and speeds up reactions<sup>3</sup> The most used solvents have high boiling points. Dimethyl formamide (DMF), diethyl formamide (DEF), MeCN, methanol, ethanol, water, and methoxy formamide or their mixtures are widely used. Under solvothermal temperatures, the starting reagents could experience unforeseen chemical alterations that are not conceivable under trivial production environment, subsequent in the production of new ligands *in situ*<sup>8</sup>

### **1.3.2 Microwave Synthesis**

Electromagnetic radiation (EMR) at frequencies between 300 and 300000 MHz is known as microwaves (MW). Only the electrical component of radiation, not its magnetic counterpart, usually affects the synthesis of chemicals. Microwave-assisted synthesis is based on the interaction of electromagnetic waves with moving electric charges. These can be electrons or ions in solids or polar solvent molecules or ions in a solution. Due to the solid's electric resistance, an electric current form inside it, which causes heating. Polar molecules in a solution attempt to associate themselves in an electromagnetic arena and an oscillating field to change their orientations over time. As a result of employing the right frequency, collisions between molecules occur, raising the kinetic energy of the system and, as a result, its temperature. MW-assisted heating is a particularly energy-efficient way of heating the solution or reactants since the radiation interacts directly with them. Thus, it is possible to achieve high heating rates and even heating throughout the sample. Since beginning materials may interact significantly with MW radiation, care must be taken to pick the proper solvents and energy input<sup>9</sup>. The first MOF

synthesized using microwave radiation is Cr-MIL-100. The chemical was produced with a 44% yield in 4 hours at 220° C under MW irradiation<sup>10</sup>. The molecular stability of the MOF-5 was improved by solvent exchange after solvothermal synthesis under microwave irradiation to increase molecular stability at feverish temperatures. Its CO<sub>2</sub> capture efficiency was then evaluated at atmospheric pressure and temperatures up to 300° C<sup>11</sup>. Both the hydrothermal approach and the microwave-assisted method were successful in synthesizing the isostructural MOF-74 (M = Ni, Mg). The technique aided by a microwave drastically cut the reaction time (from one day to one hundred minutes), and the products have smaller particles and a comparatively higher uniform distribution of particle size. higher pore textural qualities (greater micropore volume and surface area, with a comparable median pore diameter) also came into being<sup>12</sup>. Benchmark materials like UiO-66, MIL-53(Al), and HKUST-1 were produced utilizing stoichiometric amounts of reactants and with exceptional mass, space-time yields<sup>13</sup>

### **1.3.3 Mechanochemical Method**

The hunt for new, more efficient synthetic techniques has led to a resurgence of solid-state methods to chemical synthesis over the past ten years. Mechanochemistry, or chemical transformations brought or continued by mechanical force, has transformed very swiftly from a lab curiosity to a popular approach, in addition to makes chemical transformations possible in a cleaner manner but also opens completely new possibilities to produce molecules and materials as well as for molecular screening<sup>14</sup>

Two model systems are used to demonstrate the use of mechanochemical synthesis to produce metal-organic frameworks (MOFs) with large surface areas. By using a ball milling, the compounds HKUST-1, and MOF-14 were formed<sup>15</sup>. The rapid synthesis of MOF-5 with high BET area was disclosed as a practical mechanochemical technique. The impacts of variables including solvent activation, ratio of ligands, milling rate, and duration were thoroughly examined, and the improved MOF-5-B was employed to assess its ability to adsorb linear alkanes (C1–nC7)<sup>16</sup>. Using DMF as a liquid additive, a study of the reaction route for the mechanochemical production of MOF-74 from ZnO and 2,5-dihydroxyterephthalic acid (H<sub>4</sub>HDTA) was reported. Prior to MOF-74 crystallization, the complicated chemical route includes the establishment of four transient transitional stages<sup>17</sup>.

### **1.3.4 Electrochemical Method**

Both direct and indirect techniques are available for production and deposit thin films of MOF on substrates. The required MOFs are produced directly on the electrode surface via direct electrosynthesis, which includes anodic dissolution and reductive electrosynthesis. By adjusting electrochemical conditions in real time, this technique controls the production of MOFs. Through a process in which electrochemical reaction is one of the steps, MOFs are produced indirectly through electrosynthesis. Galvanic displacement, self-templated production, and electrophoretic deposition are the several implicit electrochemical processes<sup>18</sup>. Electrochemical methods for the synthesis of MOFs have numerous benefits over orthodox techniques, including quicker synthesis times, the ability to regulate the thickness and shape of the MOFs by varying the applied current or voltage, and less harsh synthesis conditions<sup>19</sup>. This study used a solution of N, N-dimethylformamide (DMF) containing 2-aminoterephthalic acid (NH<sub>2</sub>-BDC), acetic acid, and tetrabutylammonium bromide to electrochemically manufacture UiO-66-NH<sub>2</sub> using pure zirconium metal as the metal source<sup>20</sup>. HKUST-1, ZIF-8, MIL-100(Al), MIL-53(Al), and NH<sub>2</sub>-MIL-53(Al) were among the initial metal organic frameworks (MOFs) that were created in an electrochemical cell by anodic dissolution<sup>21</sup>. A quick and effective electrochemical synthesis technique in which rod-like arrays of Ni-MOFs were produced in-situ on nickel foam, which served as the source of the Ni<sup>2+</sup> ions. The end results can be used right away as a binder-free electrode material without further processing<sup>22</sup>. Utilizing an electrochemical synthesis process, HKUST-1 was created on a porous copper network. The controlled partial oxidation of the supporting mesh allowed the formation of thin crystal layers without compromising the structural integrity of the mesh<sup>23</sup>. In this study, HKUST-1 electrosynthesis employing periodic polarity reversal was investigated<sup>24</sup>.

### **1.3.5 Sonochemical Method**

Intense ultrasonic radiation (20 kHz–10 MHz) is employed in the branch of research recognized as "sonochemistry," where molecules react chemically. Acoustic cavitation is the physical phenomena that causes the sonochemical reaction. Many theories have been presented to explain how chemical bonds can be broken by 20 kHz sonic radiation<sup>25</sup>. Cu[(hfi**pb**)(H<sub>2</sub>hfi**pb**)<sub>0.5</sub>] (Cu-hfi**pb**) was produced using a sonochemical technique that yields a sizable portion of sub micrometer particles with good phase purity and a considerable yield<sup>26</sup>. Two Zr-based porphyrinic MOFs, MOF-525 and MOF-545, were made using tetrakis (4-carboxyphenyl)



porphyrin and zirconyl chloride octahydrate using a sonochemical process in 2.5 and 0.5 hours, respectively<sup>27</sup>. By using a sonochemical process and a cheap solvent called NMP (1-methyl-2-pyrrolidone), high quality MOF-177 crystals with sizes between 5 and 20 nm were successfully produced in a much shorter amount of time (40 min)<sup>28</sup>. Under ultrasonic radiation, Ni (II) nitrate hexahydrate and 1,3,5-benzene tricarboxylic acid was mixed to produce porous Ni-BTC MOF in N, N-dimethylformamide (DMF), the only solvent. It has been established that choosing the right solvent is crucial for ultrasonic treatment<sup>29</sup>

### **1.3.6 Post Synthetic Modification Method.**

Post synthetic modification (PSM) was devised and subsequently accepted by the field as a means of extending the range and adaptability of functional groups that may be integrated into MOFs. After Cohen and coworkers introduced the idea of "post synthetic modification" in 2007, some ten years after these initial studies, numerous research groups resurrected, popularized, and expanded PSM as a synthetic approach<sup>30</sup>. A helpful method for producing new metal-organic frameworks (MOFs) that can display or enhance several attributes of peer MOFs is post-synthetic modification (PSM). PSM can be conducted in several ways, including as by exchanging or adsorbing guest species, as well as by altering the linker and/or metal node. The MOF's surface environment can be transformed to add desirable features and boost structural stability. The PSM has significant potential for expanding the uses of the MOF with suitable metal or ligand<sup>31</sup>

## **1.4 Applications of MOFs**

Recently, metal-organic frameworks have drawn a lot of interest, particularly as newly created porous materials. As a result, they have an inclusive range of applications, such as materials for drug delivery, gas/vapor separation, catalysis, and storage of gases<sup>32-33</sup>

### **1.4.1 Drug Delivery Systems**

The effective distribution of drugs in the body utilizing innocuous nanocarriers is one of the biggest difficulties in drug delivery research. Governing the release and evading the "burst effect," managing matrix degradation and engineering the surface, being measurable by a variety of imaging modalities, and effectively entrapping pharmaceuticals with a high loading capacity are some prerequisites for an effective therapy using nanocarriers. In addition to these factors,

toxicity and biocompatibility are the other two important criteria for the material being evaluated as a potential novel drug carrier. The capability to modify the functional groups of the framework and tune the pore size makes MOFs ideal drug delivery materials. According to recent reports, MOFs may be crucial for drug delivery<sup>34</sup>. UiO-66 and UiO-67, two nanoscale Zr-based metal organic frameworks (MOFs), were investigated as possible anticancer drug delivery systems. Two representative pharmaceuticals—hydrophilic cisplatin and hydrophobic paclitaxel were deposited upon or inside the nano MOFs (NMOFs). To create continual release designs and lessen the harmfulness of the drugs, the drug-loaded MOFs were supplementary enclosed inside an improved poly(d-caprolactone) with d-tocopheryl polyethylene glycol succinate polymeric matrix. At a temperature of 37 °C, Simulated Body Fluid was utilized to examine physical state and release rate of the medication. It was discovered that the interaction between the medications and MOFs determines how quickly the drugs are released, whereas the microencapsulated formulations are responsible for the controlled release rates<sup>35</sup>. The hollow MOF-5 structure was produced synthetically. Its capability for drug loading and release was examined. The SK-OV-3 cell line from human ovarian cancer was used to investigate the drug loading mechanism, cytotoxicity, and cellular uptake. Zhang et al determined that the experiment successfully created a hollow MOF with an exceptional morphology, increasing the drug loading ability, achieving an idyllic result of persistent release, improving the efficacy of the treatment of a component of Chinese medicine that is hydrophobic, and providing an effective drug loading material<sup>36</sup>. Tetraethyl orthosilicate (TEOS) was added to the reaction system to produce several tiny Ti-based MOFs. Meanwhile, CCK-8 assays were used to demonstrate the produced Ti-based MOF particles' excellent biocompatibility with the L929 cell lines. Ibuprofen (IBU) was used as a model chemical to assess the Ti-based MOFs' controlled release capability<sup>37</sup>.

#### **1.4.2 Gas Separation**

The modern chemical industry relies heavily on separation and purification techniques to separate pure or purer components from complex mixtures, which represents half of all industrial energy use. Gas separation is a common step in the creation of bulk chemical products used to make fuels, resins, and polymers. Examples of this include hydrocarbon separation and natural gas processing<sup>38</sup>. Metal organic frameworks (MOFs) were incorporated into polyimide to create mixed matrix membranes (MMMs), which were then assessed for their ability to separate H<sub>2</sub>, CO<sub>2</sub>, and CH<sub>4</sub> gases. CuCo, CuNi, and NiCo doped MOF-5 nanoparticles as well as MOF-5, Cu,

Co, and Ni doped MOF-5 were created as fillers for MMMs<sup>39</sup>. A brand-new membrane for gas separation made of [Zn<sub>2</sub>(cam)2dabco] (Zn-CD) metal-carboxylate system metal-organic frameworks was created on porous ZnO substrate<sup>40</sup>. Excellent, thin MOF-5 membranes made by the secondary growth process were investigated for their permeation and separation capabilities at various feed pressures, temperatures, and feed compositions<sup>41</sup>. The novel Zn-MOF was created by adding the Fluorine moiety to tetrazolate-carboxylate ligands and coupling them with dipyriddy co-linkers<sup>42</sup>

### **1.4.3 Heterogenous Catalysis**

Heterogeneous catalysis is one of the many uses of MOFs, and it presents a constantly growing study interest because of their versatile chemical properties, distinctive pore topologies, and sizable, readily accessible core surface areas. Photocatalysis and electrocatalysis are two new forms of catalytic reactions that have emerged from the original heterogeneous catalysis over time<sup>43</sup>. It was discovered that a metal-organic framework containing palladium was a potent catalyst for the Suzuki C-C coupling, alcohol oxidation, and olefin hydrogenation processes. During catalysis, MOF configuration is maintained, and the substance is recyclable. For olefin conversion, the Pd-MOF exhibits outstanding shape-selectivity<sup>44</sup>

### **1.4.4 Sensors**

To identify hazardous compounds in the aquatic environment, four Zn-MOFs were developed under solvothermal conditions. Using a fluorescence quenching effect, fluorescence sensing tests demonstrated that four synthesized MOFs were capable of quickly and sensitively detecting hazardous ions (Fe<sup>3+</sup> and Cr<sub>2</sub>O<sub>7</sub><sup>2-</sup>), 2-Nitrophenol, and tetracycline<sup>45</sup>. A ratio metric electrochemical sensor for the measurement of several metal ions was created using metal-organic frameworks (MOFs)<sup>46</sup>. Ma et al reported the existence of the metal-organic framework [Zn<sub>2</sub>(TDPAT) (H<sub>2</sub>O)<sub>3</sub>]. As the pioneer example of a dual functional luminous sensor for quantitatively sensing the quantity of nitrobenzene and temperature, exhibits significant luminosity at normal temperature<sup>47</sup>.

### **1.4.5 Gas Storage**

Gas separation and storage are directly tied to several societal issues, including energy use, environmental preservation, and industrial output. Particularly, the storage of hydrogen and methane is necessary for the broad use of renewable energy, the separation of carbon dioxide is

essential for reducing the greenhouse impact, and the storage of poisonous gases like carbon monoxide and ammonia is indispensable for pollution regulator and the synthesis of industrial chemicals<sup>48</sup>

### 1.4.6 Water Splitting

As a crucial route for the creation of renewable energy systems, electrochemical water splitting has garnered a lot of interest. To lower their overpotentials and enable practical applications, it is urgently necessary to develop effective electrocatalysts for these processes. Numerous MOF-based/derived materials have been created that perform exceptionally well at after splitting thanks to their enormous surface area, customizable chemical components, flexible pore structure, programmable morphology, and well-defined surface functionality<sup>49</sup>. The incorporation of MOFs with PEC is believed to enhance and increase light absorption, give active sites, and regulate charge transfer dynamics due to their typical structural composition and synthetic selectivity<sup>50</sup>.

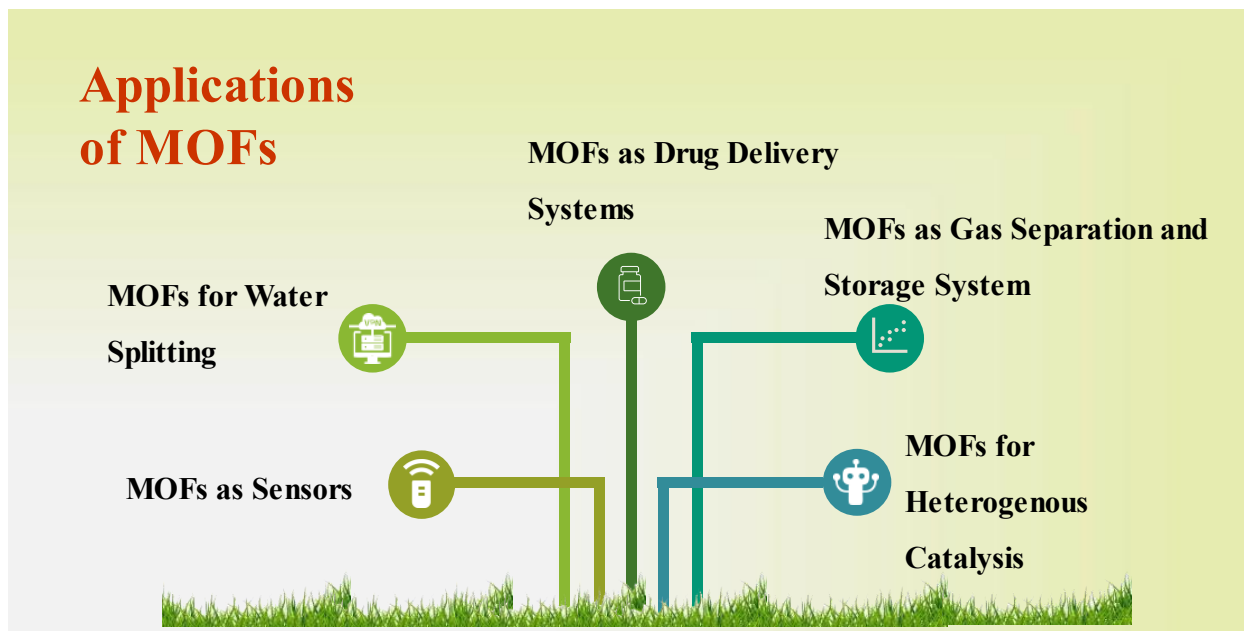


Figure 2: Applications of MOFs

## **1.5 Objectives**

- Metal organic frameworks synthesis
- Synthesis using a quick, efficient, and one-step approach.
- High current density, maximum efficiency, and long-term stability are all characteristics of newly developed catalytic materials.

## **2. Chapter 2**

### **Experimental**

#### **2.1 Materials**

##### **2.1.1 Chemicals**

All the chemicals used were pure and analytical grade. Following chemicals were used salicylaldehyde, 1, 2-phenylenediamine, 4-methyl-o-phenylenediamine, 4-aminophenol, yttrium acetate, lanthanum chloride, zinc nitrate, ethanol, dimethyl sulfoxide, and methanol.

##### **2.1.2 Instruments and Equipment**

Digital balance, hot plate, condenser, Teflon lined autoclave, centrifuge machine, and vacuum oven were used in the synthetic process of Schiff bases and their MOFs. The heating oven was used for solvothermal reaction and centrifuge machine used for washing purpose. Potentiostat was used for electrochemical studies.

## 2.2 Methodology

- Synthesis of Schiff base
- Synthesis of MOFs
- Deposition of MOFs on nickel foam
- Electrochemical water splitting

### 2.2.1 Synthesis of Schiff Bases

#### 2.2.1.1 General Procedure for Synthesis of Schiff Bases

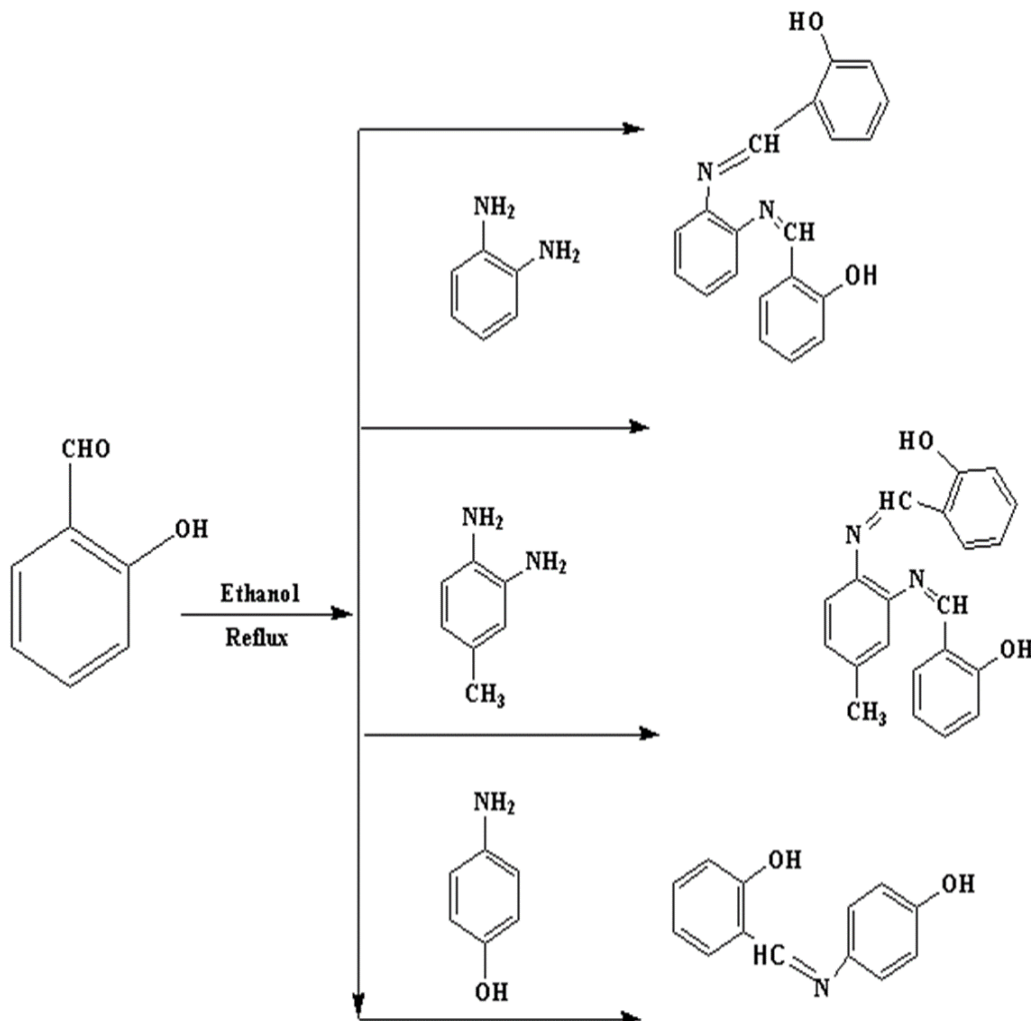
2 mmol of amine was weighed and dissolved in 5 mL ethanol in a round bottom flask. Equimolar of aldehyde was weighed and dissolved in 5 mL ethanol in a separate beaker. Then dissolved aldehyde was drop wise added to solution of amine on constant stirring. It was refluxed for 6-12 hours at a temperature of  $70^{\circ}\text{C}^{51}$ . TLC of reaction was taken after regular time intervals to monitor the progress of reaction. Extra amounts of solvents were dried by using rotary evaporator. Impurities were removed from solid products by washing them with the appropriate solvents over filter paper. By recrystallizing using ethanol as a solvent, impure products were further pure. Both open-air and vacuum ovens were used to dry the final products. Three Schiff bases were synthesized by reacting salicylaldehyde with different amines i.e., *o*-phenylenediamine, 4-aminophenol, and 4-methyl-*o*-phenylenediamine.



Figure 3: Pictorial Representation of Schiff Base Synthesis

## 2.2.2 Schiff Bases Synthesized Using Salicylaldehyde and Three Different Amines

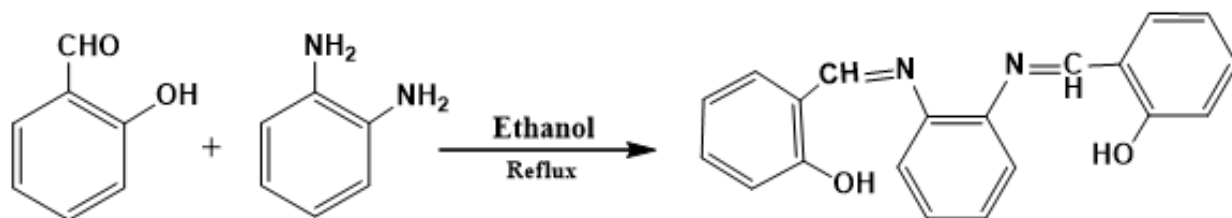
Three Schiff bases were synthesized by reacting salicylaldehyde with different amines i.e., *o*-phenylenediamine, 4-aminophenol, and 4-methyl-*o*-phenylenediamine.



*Scheme 1: Schiff Bases Synthesized using Salicylaldehyde.*

### 2.2.2.1 Schiff Base (K-1)

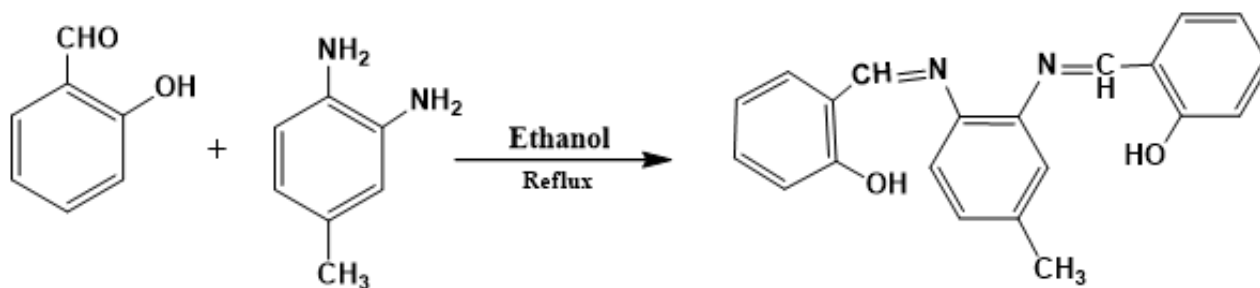
Physical appearances are orange, yield 91%, Reaction time: 4hr, M.P: 145°C, TLC system (20 % n hexane/ethyl acetate), FTIR ( $V_{\max}$ ,  $\text{cm}^{-1}$ ): 3036(C-H  $\text{sp}^2$ ), 1601(C=N), 1557(C=C-C), 1270 (C-N aromatic), 800-700 (aromatic ring), 751(1,2 disubstituted).



*Scheme 2: Synthesis of Schiff Base K-1*

### 2.2.2.2 Schiff Base (K-2)

Physical appearances are light yellow, yield 87%, Reaction time: 4hr, M.P: 140°C, TLC system (20 % n hexane/ethyl acetate), FTIR ( $V_{\max}$ ,  $\text{cm}^{-1}$ ): 3059(C-H  $\text{sp}^2$ ), 1609(C=N), 1546(C=C-C) 1287 (C-N aromatic), 800-700 (aromatic ring).

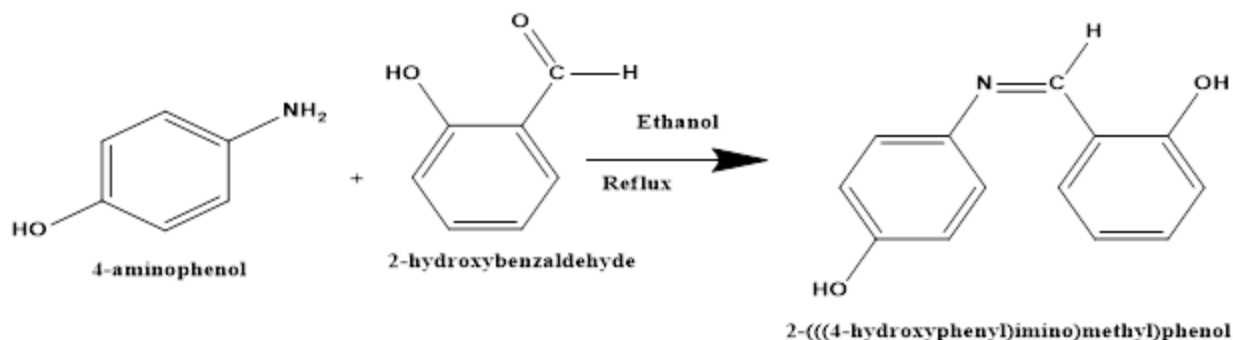


*Scheme 3: Synthesis of Schiff Base (K-2)*

### 2.2.2.3 Schiff Base (K-3)

Physical appearances are brownish dark, yield 80%, Reaction time: 5 hr, M.P: 155°C, TLC system (20 % n hexane/ethyl acetate), FTIR ( $V_{\max}$ ,  $\text{cm}^{-1}$ ): 3200(O-H intermolecular bonded), 1613(C=N), 1506(C=C-C), 1250 (C-N aromatic), 1209(C-O phenol), 800-700 (aromatic ring) 751(1,2 disubstituted).





*Scheme 4: Synthesis of Schiff Base (K-3)*

## 2.2.3 Synthesis of MOFs

### 2.2.3.1 General Procedure for Synthesis of MOFs

The reported method was used to synthesize MOFs<sup>52</sup>. 1 mmol of metal salt, 0.5 mmol of Schiff base and terephthalic acid were weighed and dissolved in 25 mL DMSO. And continuously stirred for 30 minutes to produce a homogeneous solution. Following that, this solution was put into a 30 mL Teflon-lined autoclave and heated for 24 hours at 160° C. The autoclave was cooled to room temperature. For washing, the solution was poured into falcon tubes and centrifuged for 10 minutes at 8000 rpm. The solution was kept in a vacuum oven for drying then rinsed with methanol four to five times.

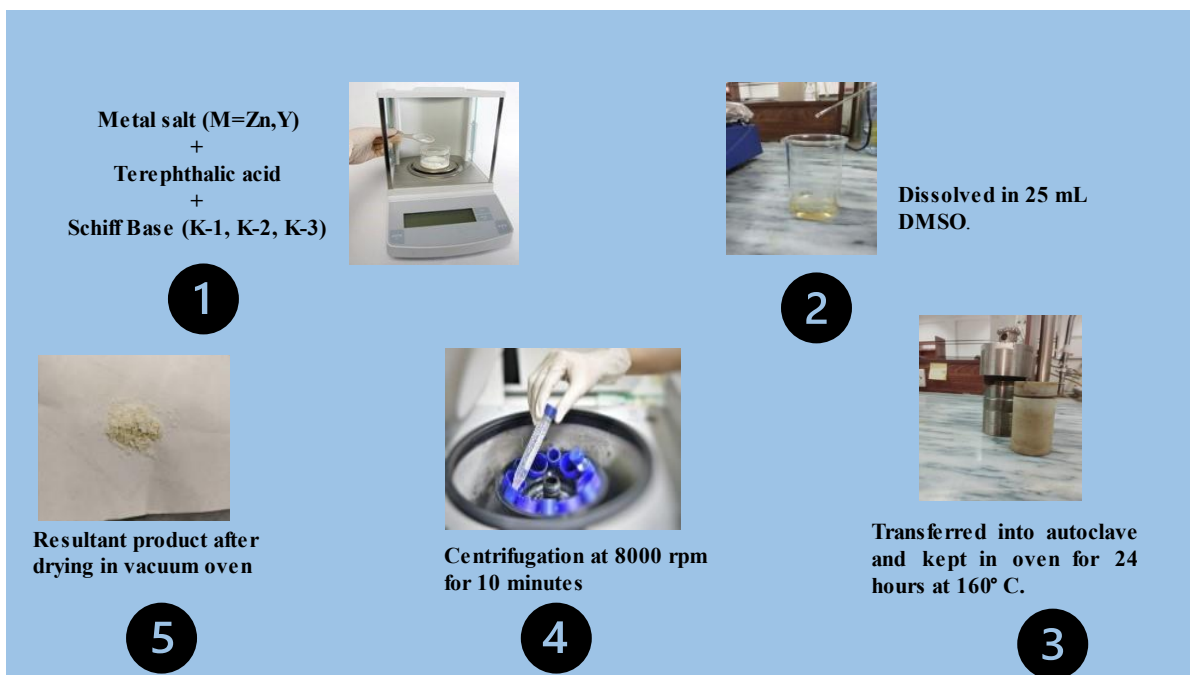


*Figure 4: Schematic Representation of MOF Synthesis*

#### **2.2.4 Electrode Formation**

A material slurry was prepared, evaluated with several solvents, and the results were evaluated. Analytical grade DMSO was chosen as the solvent for the entire study since it demonstrated the best material dispersion. A 10 mL glass vessel containing 2 mL of ethanol and 10 mg of each substance was used to create the slurry. To create a correct dispersion for better electrode production, the ink was ultrasonically treated for 30 minutes at high sound pressure. For full dispersion, the sonicator bath was maintained at 60°. The substance was then dropped onto the nickel foam using a micro pipette with a thin needle-like tip. Material was applied on nickel foam two to three times to form a homogenous layer.

#### **2.2.5 Electrochemical Water Splitting**

The Gamry Interface 1000 Potentiostat workstation was used to do electrochemical study. On this device, employing a three-electrode setup, all the studies were conducted.

The first is a cathode-functioning electrode containing synthesized substance deposited on the nickel foam surface. The second is a counter electrode, which consists of platinum wire acting as an anode. The third one is the reference electrode, whose major function is to measure the potential provided to the system and the following voltage used on the working electrode. To get better results, a unique electrochemical cell was devised. An electrolyte volume of 30 mL may fit inside the cell. The cell, in which the three-electrode assembly was mounted, was covered with a white Teflon top with three holes. The primary purpose of cell was to maintain minimal space between the electrodes while maintaining the electrode system closed. This electrochemical cell was thoroughly cleaned using ethanol and deionized water before use. The platinum wire was also immersed in a 20% nitric acid solution for the good results. Several tests that are required for the evaluation of the data were conducted in electrochemical water splitting. Chronopotentiometry (CP), Linear sweep voltammetry (LSV), Potentiostat Electrochemical Impedance Spectroscopy (EIS), and Cyclic Voltammetry Test (CV) were among those tests. These experiments were conducted to collect various data and afterwards confirm the various synthesized materials, as well as to facilitate comparison study.

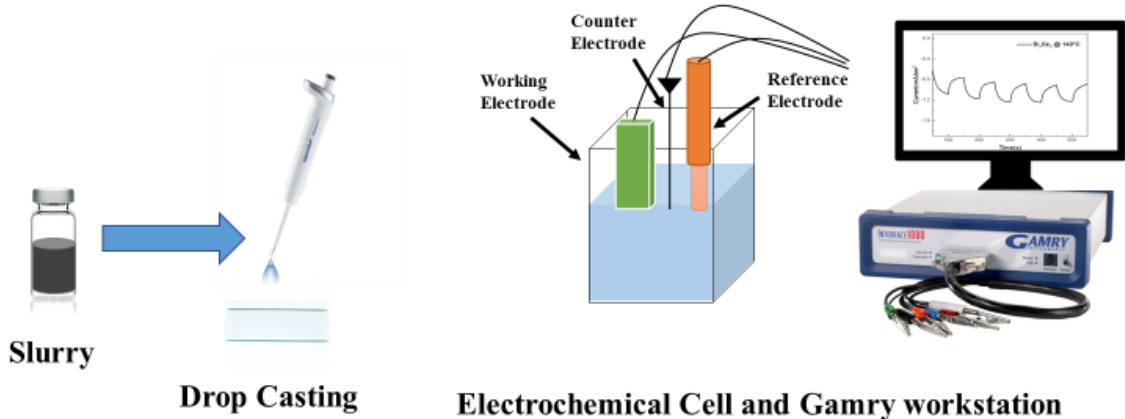


*Figure 5: Electrode Formation and Electrochemical Setup*

## 2.3 Characterization Techniques

It is crucial to characterize the material for a certain application. Applications and activity of the material are unnecessary without proper and prior understanding of the material's size, shape, morphology, crystal structure, and elemental analysis. Numerous characterizations have been conducted for this reason to learn about all the criteria mentioned above regarding the material. The following paragraphs of this chapter will discuss each of those in depth.

### 2.3.1 X-ray Diffraction

X-ray diffraction is a flexible technique that offers information about crystalline materials. The average grain size, crystalline structure, strain, crystal defects, and phase composition can all be learned about by examining the diffraction pattern. To comprehend how a material was created or treated, one might look at the crystal textures, which describe the preferred orientations of crystalline grains inside the material. Insights into how the material's properties might be optimized for purposes are available from the determination of crystal's optimal orientations. Additionally, XRD enables the examination of crystal flaws and imperfections. Researchers can determine the existence of lattice strain, which can result from a variety of reasons like impurities, defects, or external stressors, by studying peak broadening or splitting. Understanding the material's mechanical, electrical, or optical characteristics requires this information. In numerous scientific and technological disciplines, such as materials science, chemistry, geology,

and solid-state physics, this knowledge is essential for comprehending the characteristics and behavior of materials<sup>53</sup>.

### **2.3.2 Scanning Electron Microscopy**

One of the most prominent methods, scanning electron microscopy (SEM), may image the substance with a resolution of only a few nanometers<sup>54</sup>. An electron focused beam of high energy is employed by an electron scanning microscope for the creation of distinct types of signals at the surface of sample. The signals from backscattered electrons (BSE) and secondary electrons (SE) are investigated and asserted. SEM is used to reveal a variety of sample characteristics, including chemical composition, surface appearance, crystalline structure, and more. The beam is scanned, and data is collected, on predetermined regions of the sample surface<sup>55</sup>.

### **2.3.3 Energy Dispersive X-ray Spectroscopy**

Energy dispersive X-ray analysis was used to chemically characterize and elementally analyze the samples. The sample that included varying elemental proportions was in contact with the X-ray during this characterization process. The characteristic X-rays that a specimen emits serve as the foundation for EDX. When an elemental analysis of a sample is performed using EDX, a spectrum is created that displays the peaks related to the sample's elements composition. By utilizing Moseley's law to determine the percentage of the elements contained in the compounds, peak positions can be predicted. This characterization method allowed us to determine the purity of the synthesized substance. Additionally, one can create elemental mapping utilizing this characterization technique<sup>56</sup>.

### **2.3.4 Fourier Transform Infrared Spectroscopy (FTIR)**

The FTIR technique may detect the absorption or emission of infrared light by a solid, liquid, or gas. To get high spectral resolution data using FTIR, a broad wavelength range can be used, typically between 5000 and 400  $\text{cm}^{-1}$  for the mid-IR region and between 10,000 and 4000  $\text{cm}^{-1}$  for the near-IR region<sup>57</sup>.

### **2.3.5 Electrochemical Studies**

1.0 M KOH solution serves as the electrolyte in a three-electrode cell assembly, the electrocatalytic response of the catalysts was investigated on the Gamry Potentiostat at room temperature. Ag/AgCl obliged as the reference electrode, Pt wire served as the counter electrode, and a catalyst that had been coated on NF served as the working electrode.

### 2.3.6 Calculation of Over Potential

Based on the reverse linear sweep voltammetry scan, over potential was determined. It is determined using a current density of 10 mA. The chosen value of  $10 \text{ mAcm}^{-2}$  was then subtracted from the 1.23 V thermodynamic water splitting value.

$$1.57 - 1.23 = 0.34 \text{ V}$$

$$0.32 * 1000 = 340 \text{ mV}$$

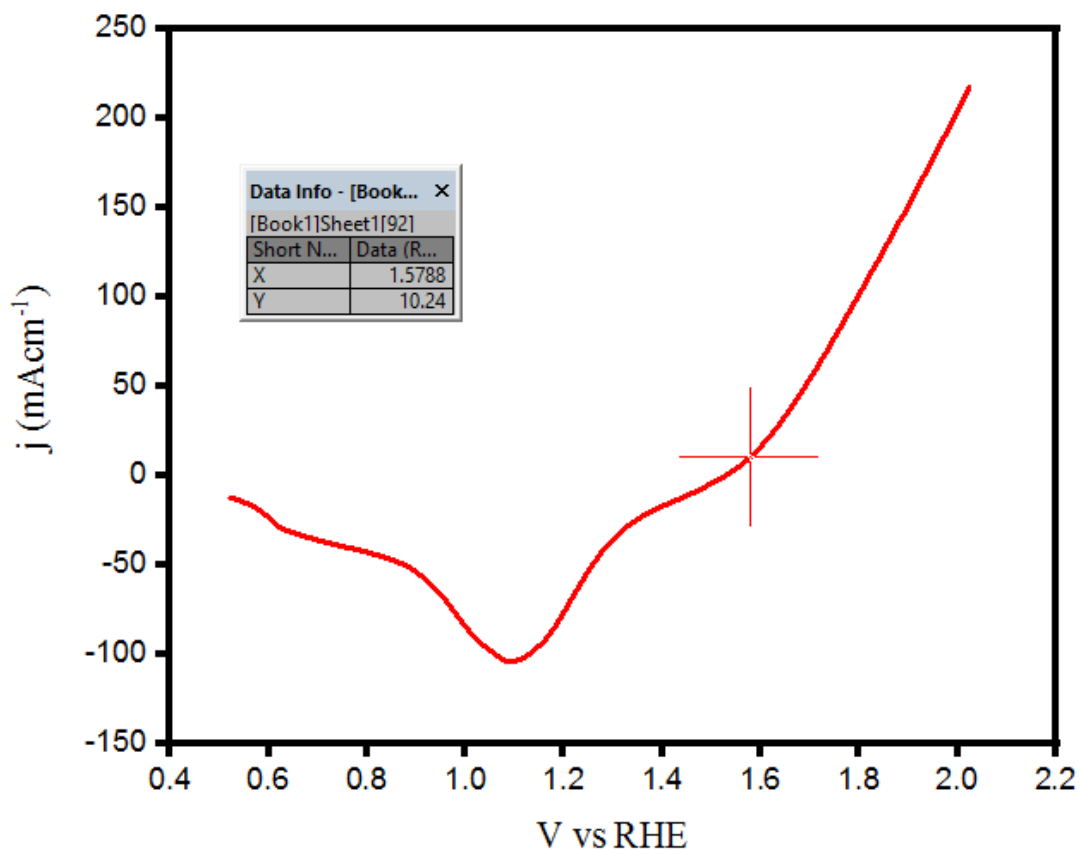


Figure 6: Reverse LSV of Zn-MOF for Calculating Overpotential

### 3. Chapter 3

#### 3.1 Results and Discussion

##### 3.1.1 Characterization of Schiff Base K-1

###### 3.1.1.1 FT-IR analysis

The absence of bands at  $1735\text{ cm}^{-1}$  due to carbonyl (C=O) and the emergence of a significant new band at  $1601\text{ cm}^{-1}$  due to the azomethine, (HC=N) linkage were viewed in the FT-IR spectrum of Schiff base ligand (K-1). The presence of this new band indicated that Schiff base has successfully synthesized<sup>58</sup>. The band present at  $3036\text{ cm}^{-1}$  ascribed to C-H ( $\text{sp}^2$ ) stretch. At  $1557\text{ cm}^{-1}$  the C=C IR band was visible, while at  $1270\text{ cm}^{-1}$ , the C-N stretch was detected.

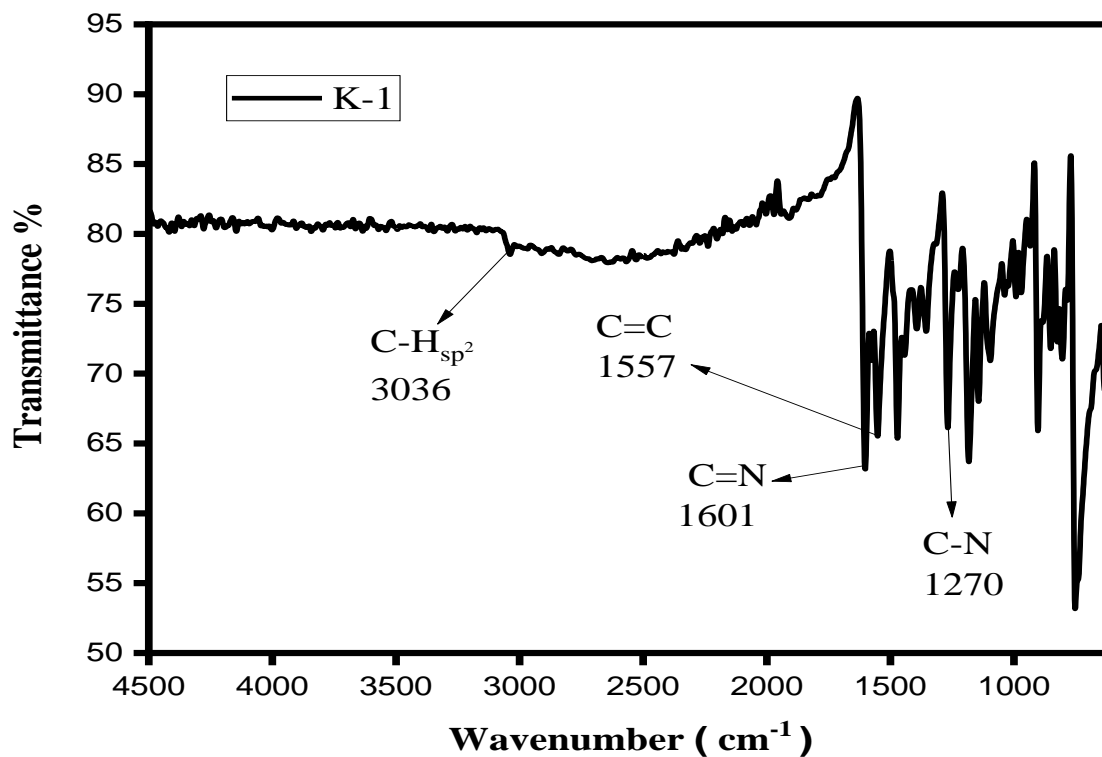


Figure 7 : FT-IR spectrum of Schiff Base (K-1)

###### 3.1.1.2 CHN analysis

The elemental analysis of the synthesized Schiff base was obtained using CHN analysis. The percentages of the product that were calculated and discovered are listed in the table below, and they are very similar, supporting the synthesis of the Schiff base.

Table 1: CHN Analysis of Schiff Base (K-1)

Code	Calculated %			Found %		
	C %	H %	N %	C %	H %	N %
K-1	84.39	5.64	9.85	84.27	5.51	9.63

### 3.1.2 Characterization of Schiff base K-2

#### 3.1.2.1 FTIR analysis of K-2

The presence of IR band at  $1609\text{ cm}^{-1}$  indicated the formation of Schiff base. The C=C aromatic stretch was present at  $1546\text{ cm}^{-1}$ , while C-H ( $\text{sp}^2$ ) showed band at  $3059\text{ cm}^{-1}$ . The band  $1287\text{ cm}^{-1}$ , there was a C-N single bond stretch.

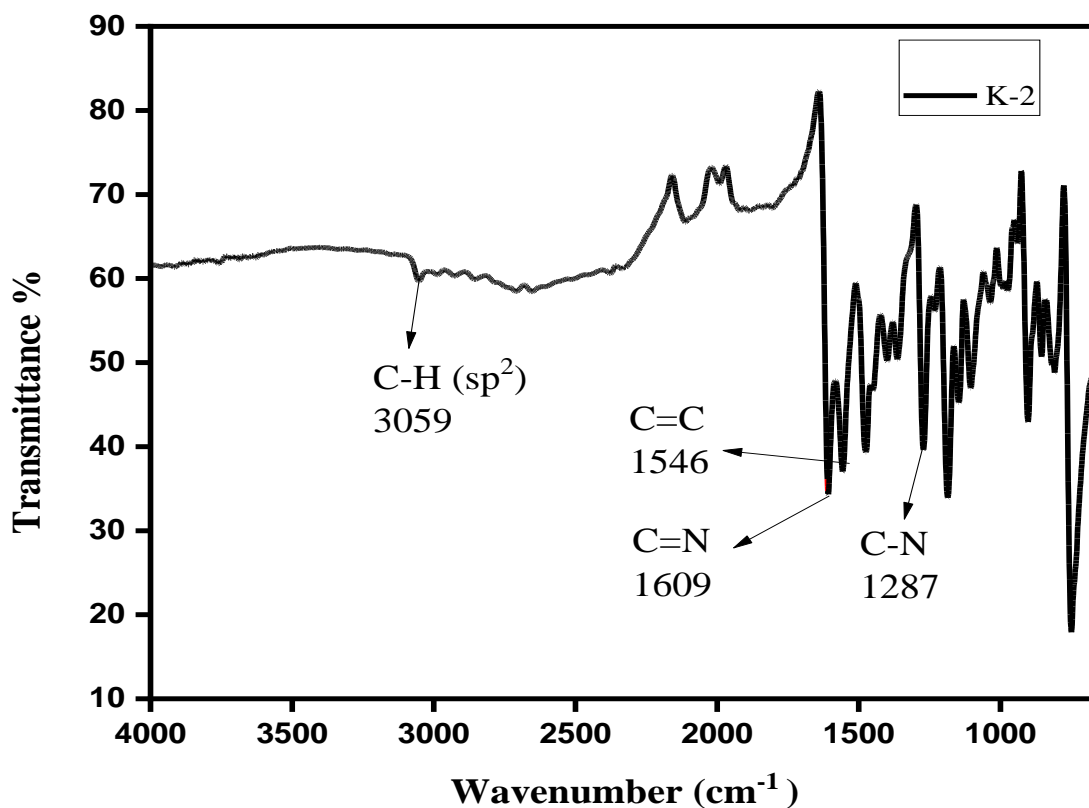


Figure 8: FT-IR spectrum of Schiff base (K-2)

### 3.1.2.2 CHN Analysis

Using CHN analysis, it was possible to find out the percentage composition of the synthesized Schiff base. As can be noticed from the table below, the calculated and discovered product percentages are remarkably similar, validating the formation of the Schiff base.

*Table 2: CHN Analysis of Schiff base (K-2)*

Code	Calculated %			Found %		
	C %	H %	N %	C %	H %	N %
K-2	84.54	6.05	9.38	84.27	6.00	9.25

### 3.1.3 Characterization of Schiff Base K-3

#### 3.1.3.1 FT-IR analysis

The FT-IR spectrum of Schiff base K-3 was shown in the figure 9. The characteristics band represented by azomethine linkage was present at  $1613\text{ cm}^{-1}$ . This indicated the successful formation of Schiff base ligand.



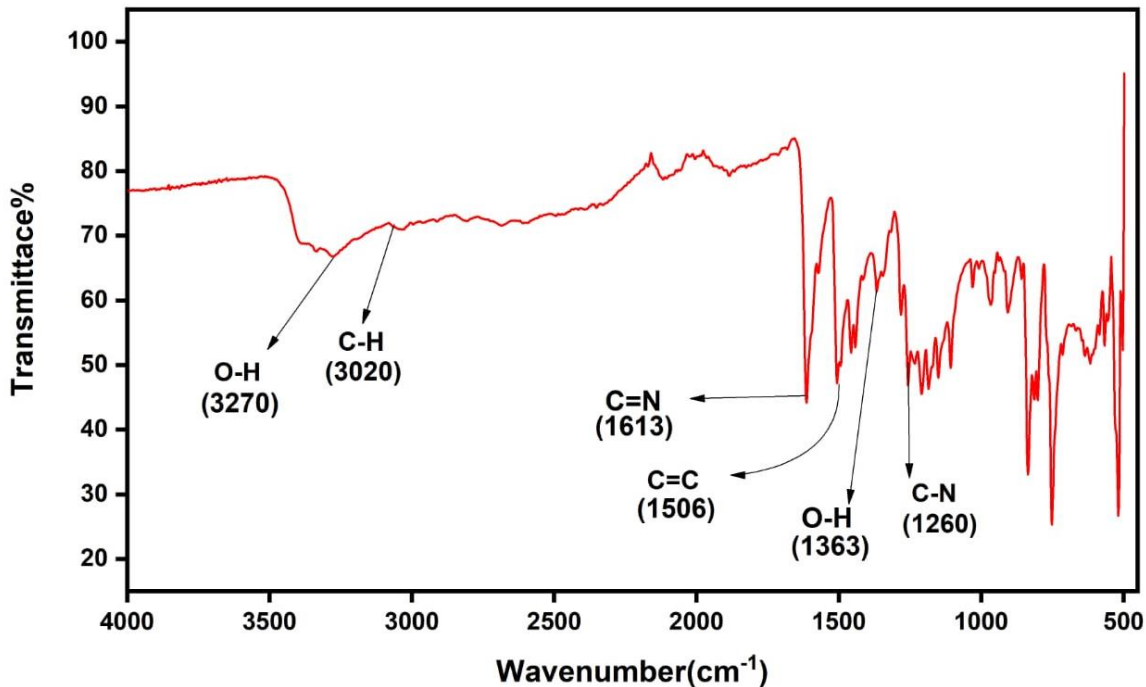


Figure 9: FT-IR Spectrum of Schiff base (K-3)

### 3.1.3.2 CHN analysis

The calculated and found percentage composition of carbon, hydrogen and nitrogen was given in the table below. The found percentage was done using elemental analyzer.

Table 3: CHN of Schiff base (K-3)

Code	Calculated %			Found %		
	C %	H %	N %	C %	H %	N %
K-2	86.06	6.09	7.72	86.01	6.04	7.53

### 3.1.4 Characterization of Zn-MOF

A straightforward solvothermal approach was used to synthesize the Zn-MOF. The Zn (NO<sub>3</sub>)<sub>2</sub>.6H<sub>2</sub>O, Schiff base (K-2) and terephthalic acid were added in a 2:1:1 ratio to the Teflon-lined autoclave. Then, XRD, FT-IR, SEM, EDX, and TGA were used to characterize the synthesized MOF.

### 3.1.4.1 FTIR of Zn-MOF

Novel synthesized Zn-MOF was characterized by FT-IR. The IR band present at  $1491\text{ cm}^{-1}$  attributed to imine linkage of Schiff base which is shifted from  $1609\text{ cm}^{-1}$  to  $1491\text{ cm}^{-1}$ , this shifting is due to the linkage of Schiff base precursor with the metal cluster ion. As for -BDC, the distinctive bands of  $\text{H}_2\text{BDC}$   $1686\text{ cm}^{-1}$  are not seen, evidence that the  $\text{H}_2\text{BDC}$  was fully deprotonated during the reaction and functions as the bridging ligand to produce Zn-MOF<sup>59</sup>. The product shows the successful coordination of zinc ion and  $\text{BDC}^{2-}$  ligands by exhibiting new bands  $1618\text{ cm}^{-1}$  asymmetric stretching vibrations of  $-\text{COO}^-$ ;  $1387\text{ cm}^{-1}$ , symmetric stretching vibrations of  $-\text{COO}$ ; and  $750\text{ cm}^{-1}$ , ring-out-of-plane vibration of the 1,4-substituted benzene ring of the linkers. The band present at  $1247\text{ cm}^{-1}$  ascribed to the C-N stretching vibration.

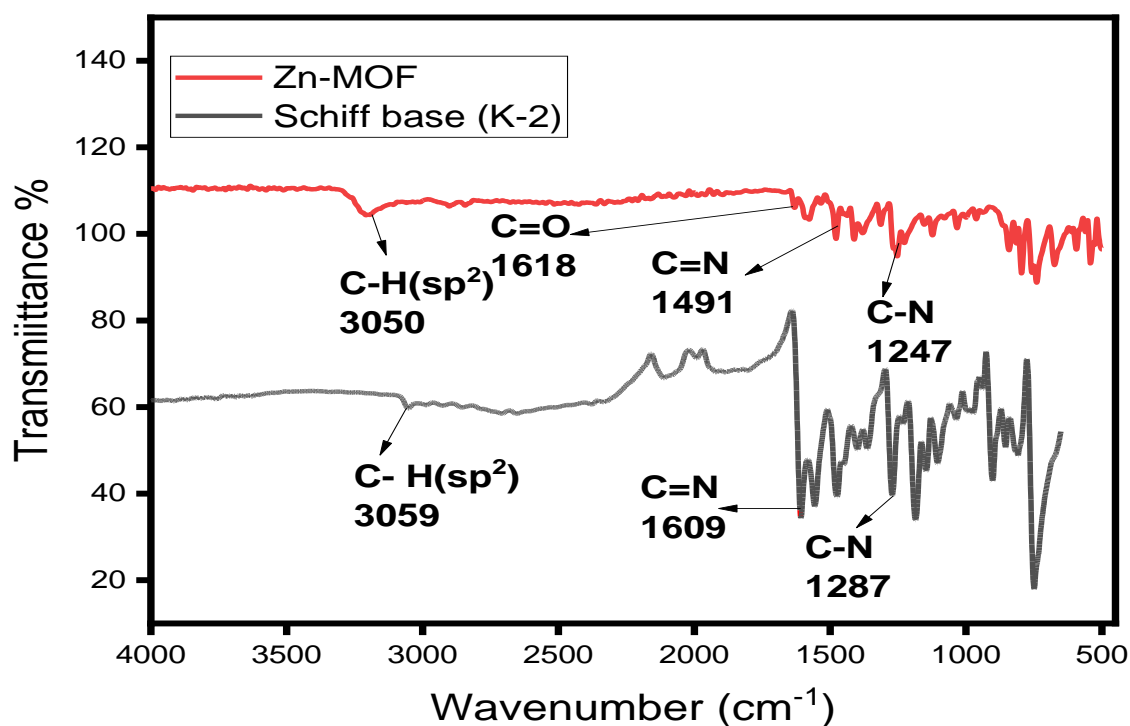
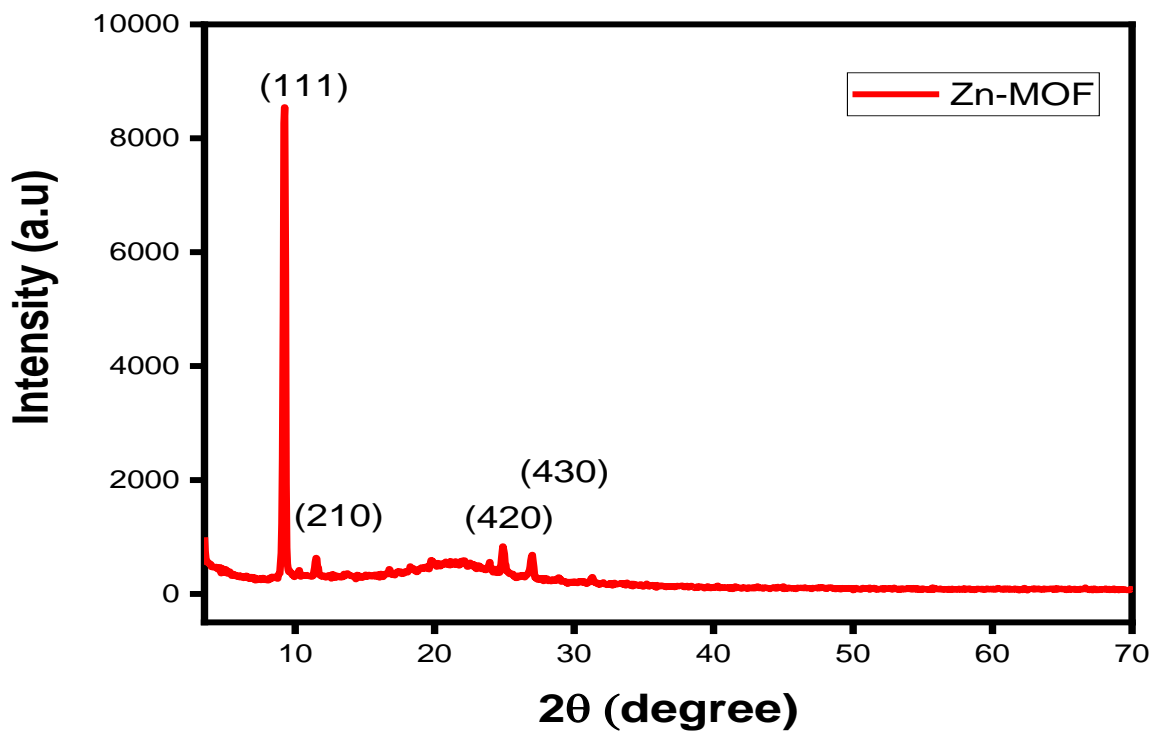


Figure 10: FTIR Spectrum of Zn-MOF/Schiff base (K-2)

### 3.1.4.2 XRD of Zn-MOF

The XRD pattern of as synthesized Zn-MOF was presented in the figure 11. The XRD pattern of Zn-MOF distinctly demonstrated well-defined diffraction peaks, showing the crystalline

structure of the material. The XRD pattern of the Zn-MOF showed 4 distinct peaks. The peak at  $9.2^\circ$  confirmed the successful formation MOF.



*Figure 11: XRD of as synthesized Zn-MOF*

#### **3.1.4.3 SEM of Zn-MOF**

Scanning electron microscopy was used to govern the topography and surface morphology of synthesized Zn-MOF. Figure 12 showed the SEM images of MOF at different resolution. The shape of Zn-MOF resembles that of nano flakes, as can be seen in the SEM images.

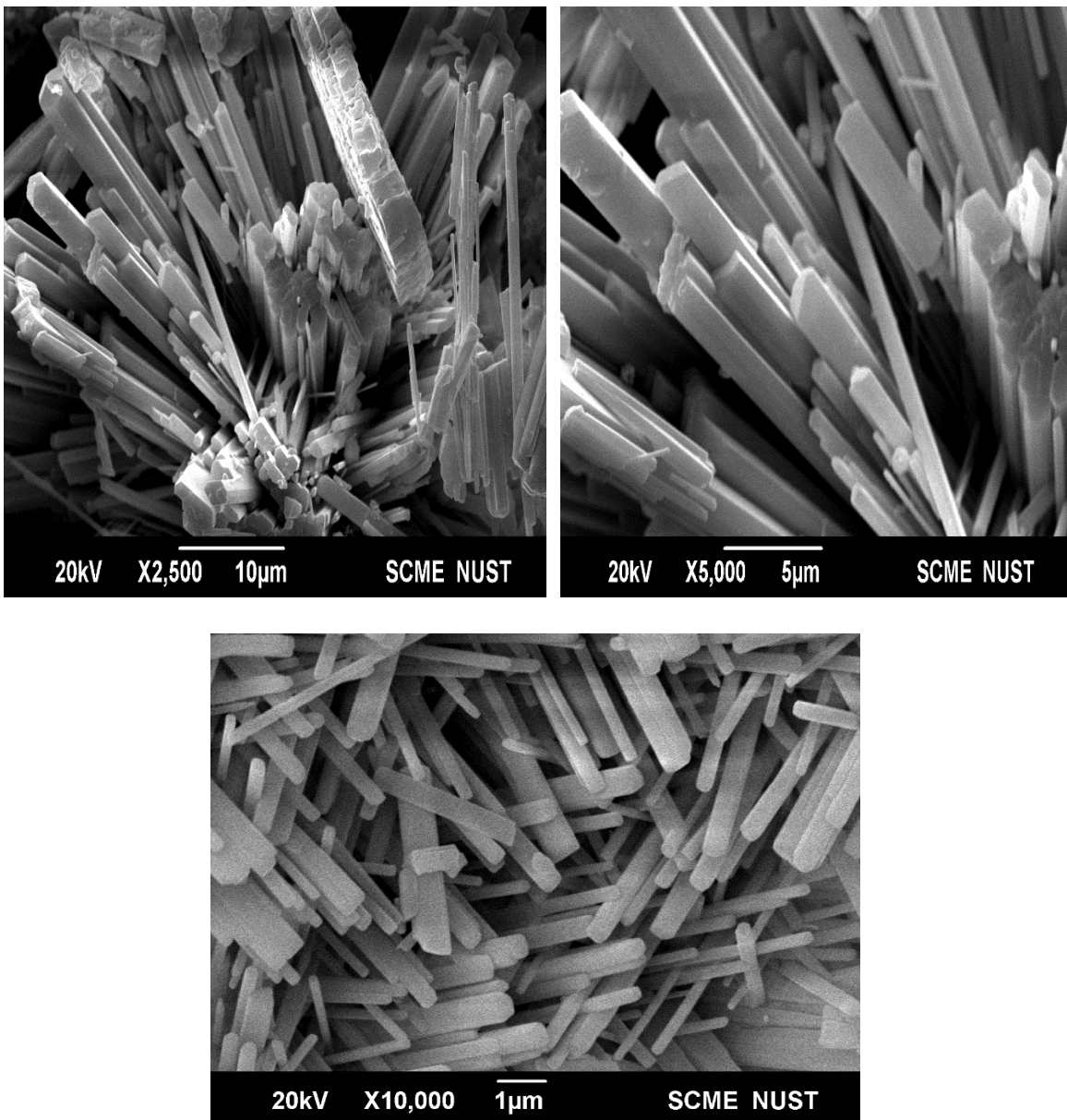


*Figure 12: SEM Images of Zn-MOF at Different Resolutions*

#### **3.1.4.4 EDX of Zn-MOF**

The elemental makeup of the Y-MOF (1) was examined using energy-dispersive X-ray spectroscopy (EDX). Carbon (C), oxygen (O), nitrogen (N), and zinc (Zn) were found in the MOF, according to the ensuing EDX spectra. These components show that the MOF was effectively synthesized in addition to it includes the desired ingredients. The EDX spectrum was displayed in Figure 13 clearly identifies the peaks that are unique to each element, showing that it is present in the MOF.

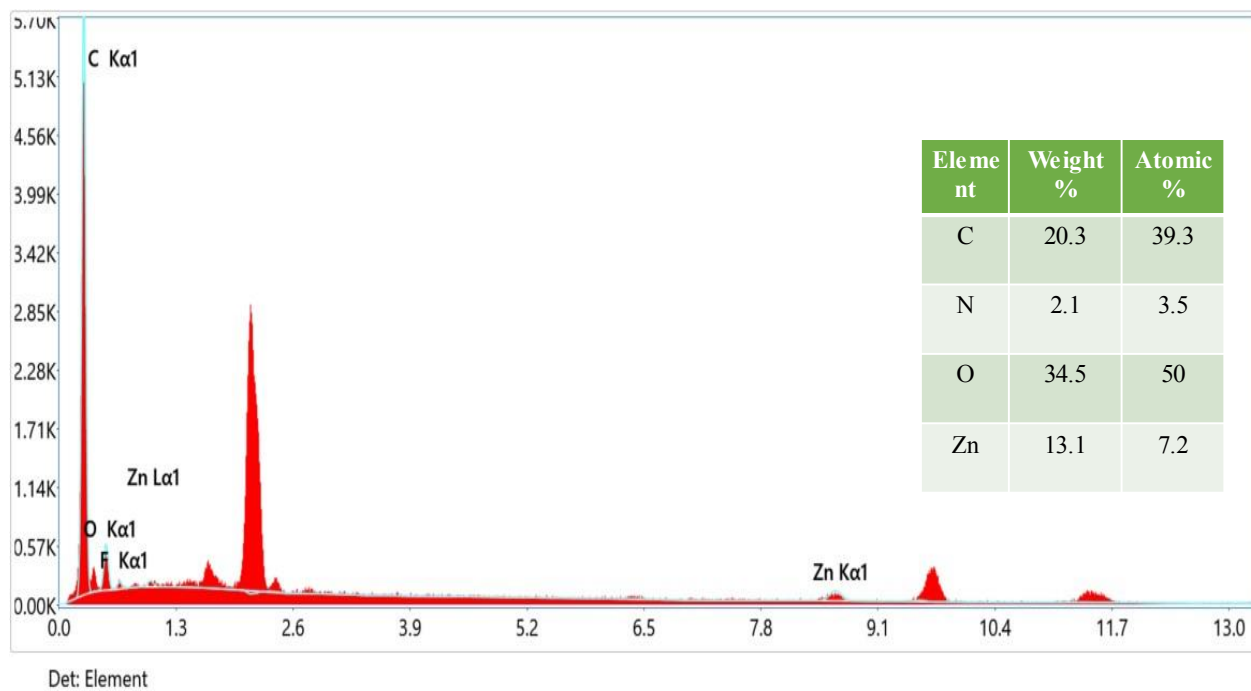


*Figure 13: EDX of Zn-MOF*

#### **3.1.4.5 TGA of Zn-MOF**

Thermal gravimetric analysis was used to assess the thermal stability of the as-synthesized Zn-MOF. The TGA profile of Zn-MOF was shown in the figure 14. TGA profile depicted that total weight loss is 68.25 %. The thermogram showed that first weight loss initiated at temperature of 102 °C. the weight loss up to 330 °C was due to the solvent and water molecules. The weight loss above 330 °C was mainly due the organic ligand attached to metal cluster.

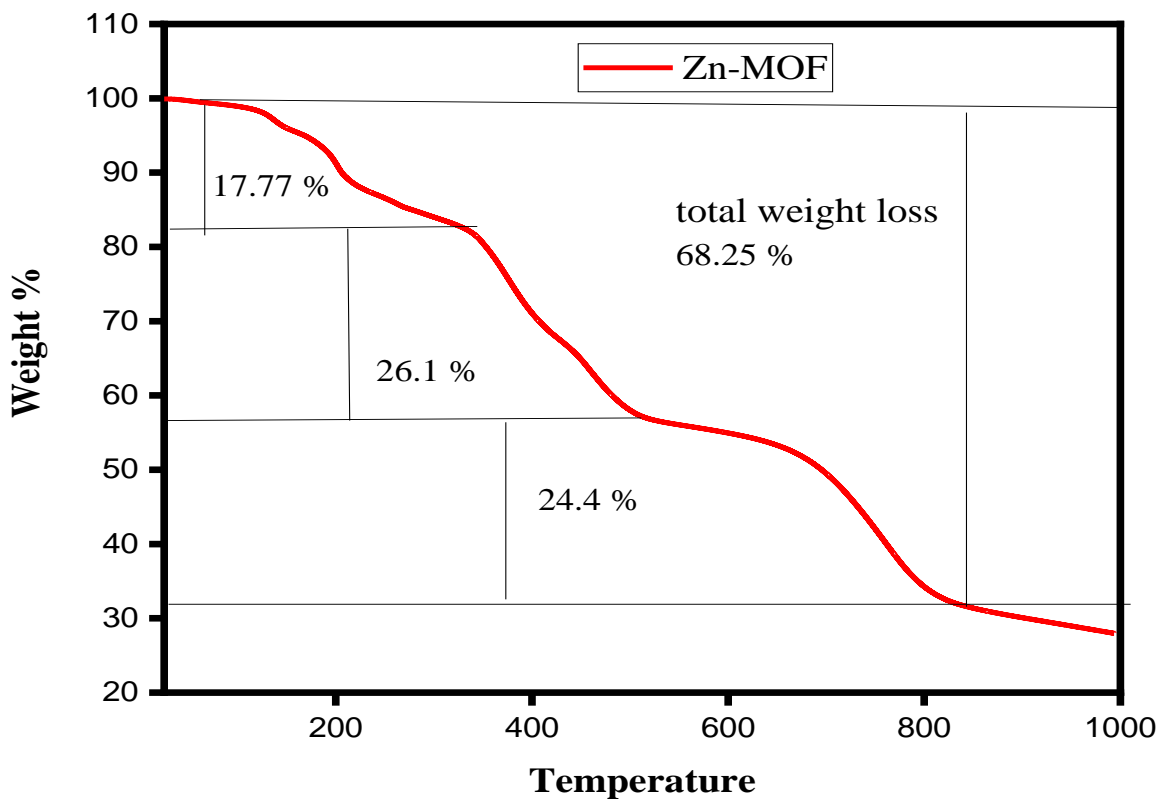


*Figure 14: TGA of Zn-MOF*

### 3.1.5 Characterization of Y-MOF (1)

#### 3.1.5.1 FT-IR of Y-MOF (1)

The absence of the distinguishing band of protonated carboxyl group ( $1730-1700\text{ cm}^{-1}$ ) in the FT-IR spectrum indicated that the  $\text{H}_2\text{BDC}$  has entirely lost its proton throughout the reaction and is now acting as the connecting ligand to create Y-MOF<sup>60</sup>. The band present at  $1550$  and  $1365\text{ cm}^{-1}$  corresponds to asymmetric and symmetric stretching vibrations of  $-\text{COO}^-$  in the spectrum. The band present at  $1500\text{ cm}^{-1}$  attributed to the azomethine linkage of the Schiff base precursor.

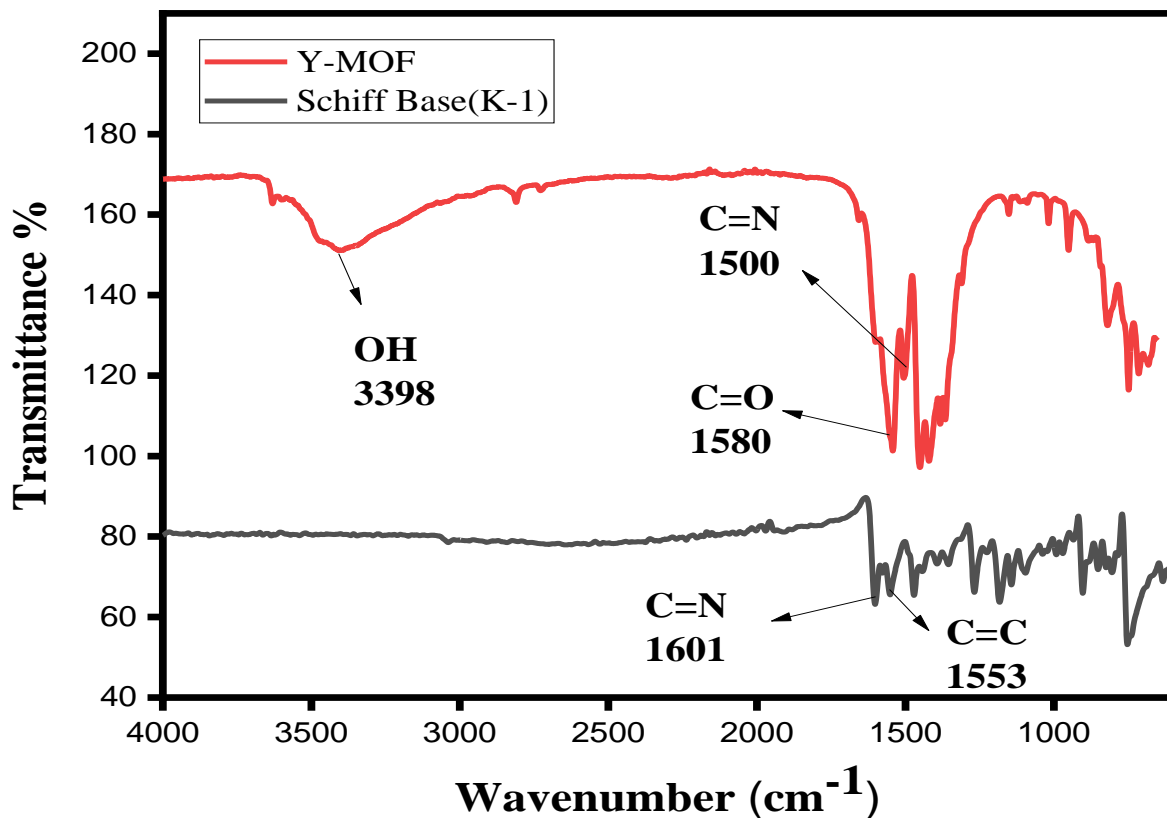


*Figure 15: FT-IR of Y-MOF (1)/ Schiff base (K-1)*

### 3.1.5.2 XRD of Y-MOF (1)

There were eight distinct peaks in the Y-MOF XRD pattern. The peak observed at  $6.3^\circ$  indicates that the MOF was successfully formed. The crystalline structure of the synthesized Y-MOF (1) was confirmed by presence of sharp and distinctive peaks in the XRD pattern.

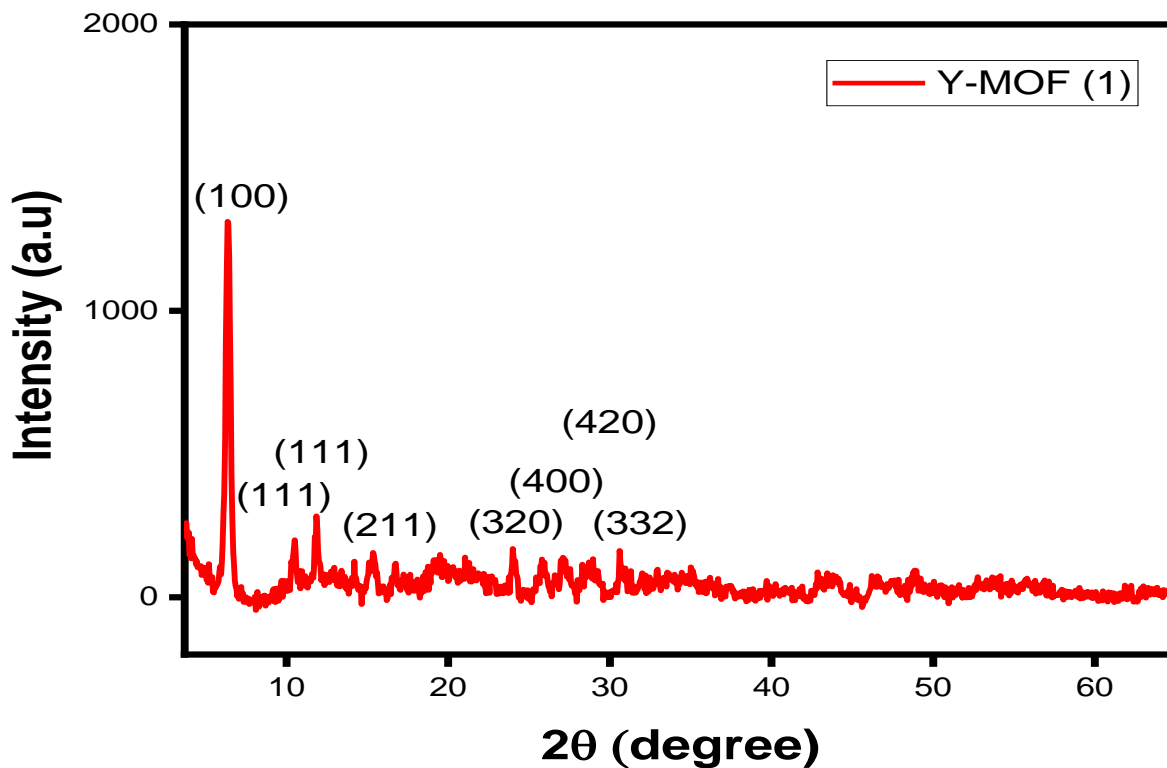


*Figure 16: XRD of Y-MOF (1)*

### **3.1.5.3 SEM of Y-MOF (1)**

The surface morphology and topography were assessed by scanning electron microscopy. The SEM images of Y-MOF (1) showed in the figure. The figure 17 showed that the Y-MOF (1) has flakes like morphology. The flakes-like morphology of the MOF can be traced to its crystal structure, might have a layered or plate-like pattern of the constituent building blocks that comprise the MOF. The flakes-like form may have a large surface area that is conducive to catalytic activation. The high surface area can give greater potential sites for the catalytic process to occur, leading to better catalytic performance.



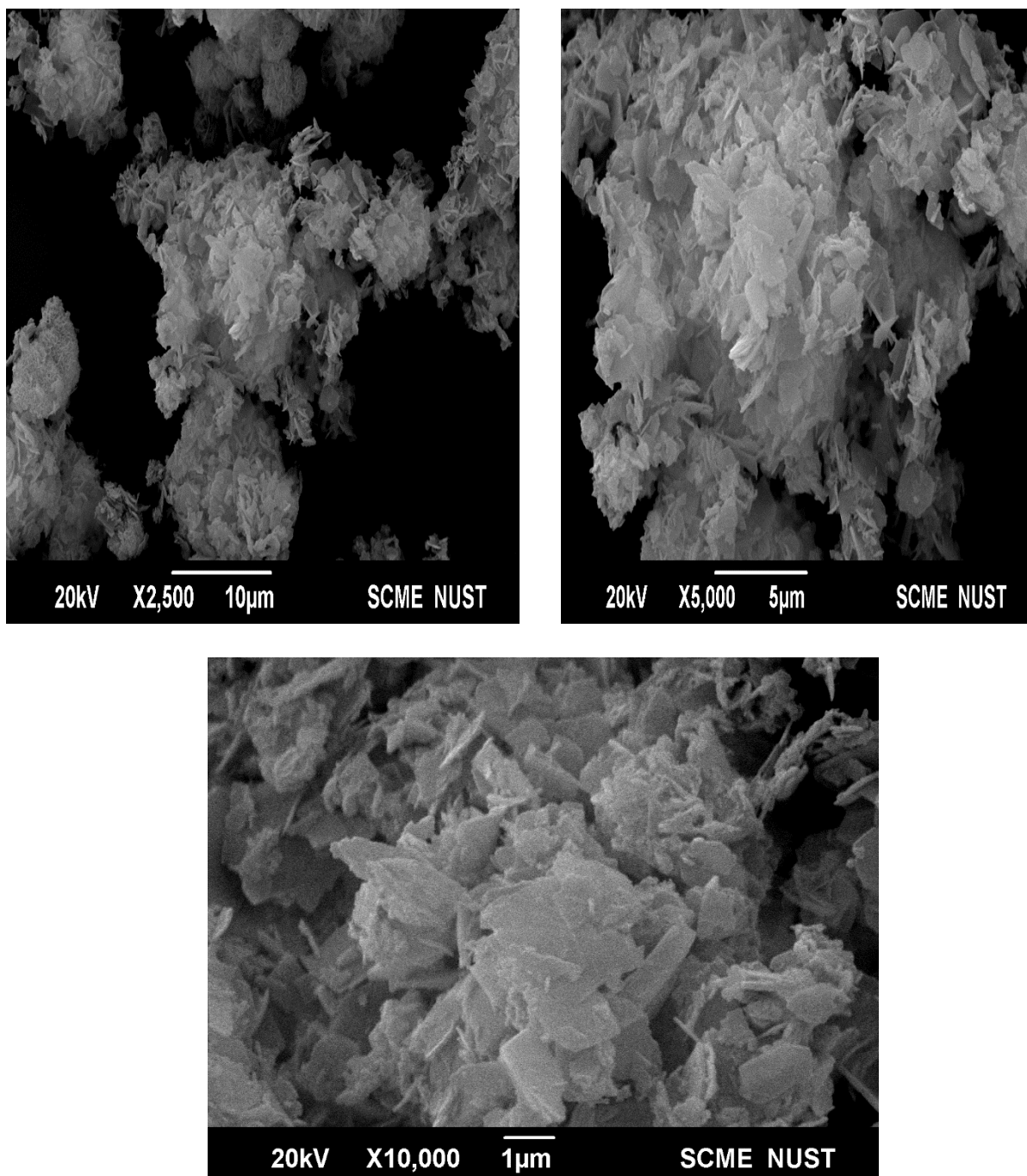


*Figure 17: SEM Images of Y-MOF (1) at Different Resolution*

#### **3.1.5.4 EDX of Y-MOF (1)**

The elemental composition of the synthesized Y-MOF (1) was confirmed using an Energy Dispersive X-ray Spectroscopy (EDX) investigation. The obtained EDX spectrum (figure 18) unmistakably shows that the MOF contains the elements carbon (C), oxygen (O), nitrogen (N), and yttrium (Y). The existence of these elements in the MOF was clearly demonstrated by the

detection of them at typical energy levels. This proves that the Y-MOF (1) was successfully synthesized and offers information on its elemental make-up.

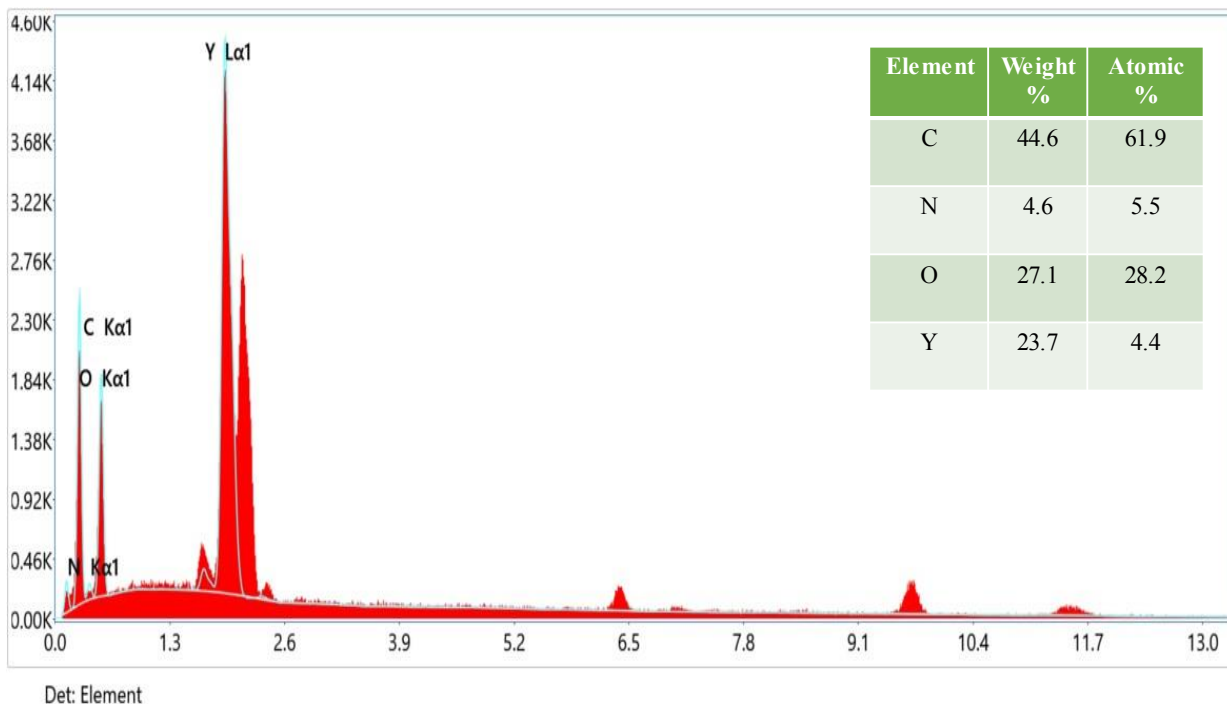


*Figure 18: EDX of Y-MOF (1)*

### 3.1.5.5 TGA of Y-MOF (1)

In figure 19, the Y-MOF (1) TGA thermogram was displayed. About 49.81% of the total weight was lost. The thermogram showed that the weight loss happened in three phases that followed each other. The first weight reduction was about between 25 and 150 °C. Between 150 and 390 °C, the second phase of weight loss was carried out. And the final weight stage began at 390 °C and continued up to 650 °C.

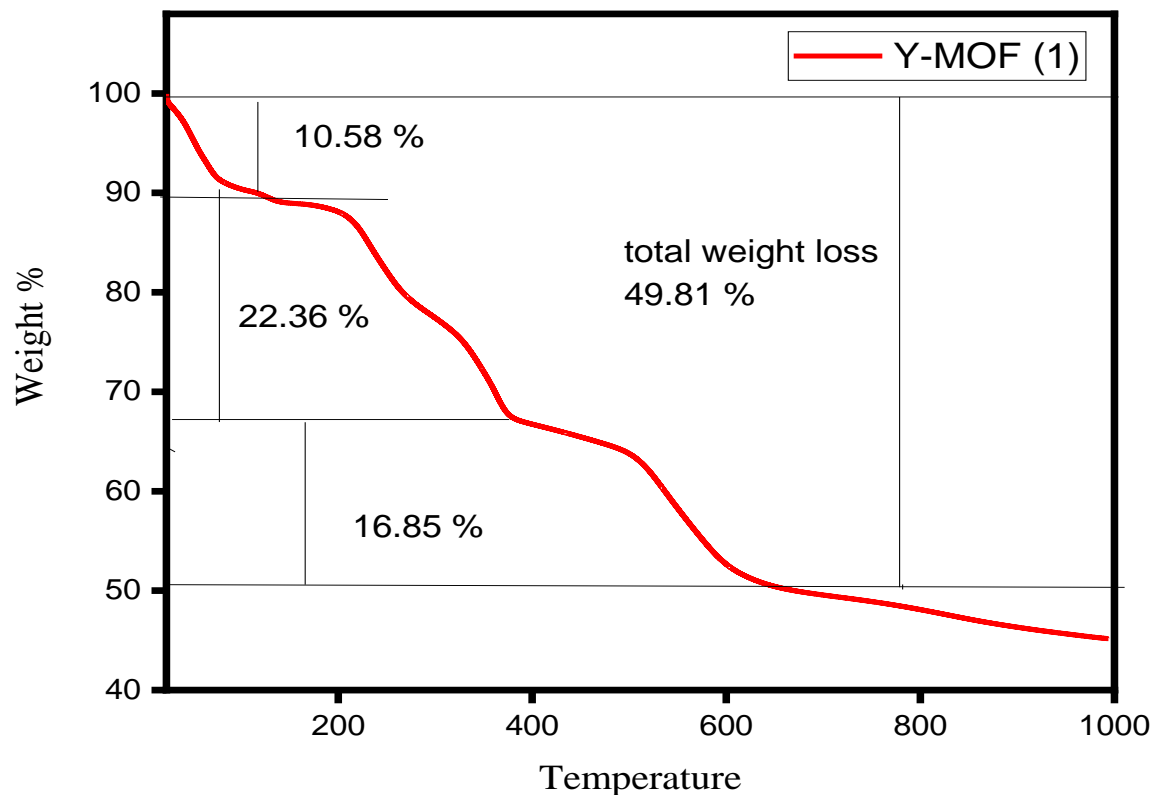


*Figure 19: TGA of Y-MOF (1)*

### 3.1.6 Characterization of Y-MOF (2)

#### 3.1.6.1 FT-IR of Y-MOF (2)

Since the FT-IR spectrum lacks the characteristic bands of protonated carboxyl groups ( $1730\text{-}1700\text{ cm}^{-1}$ ), it is possible that the  $\text{H}_2\text{BDC}$  is now acting as a bridging ligand to create Y-MOF. The bands at  $1640$  and  $1375\text{ cm}^{-1}$  in the spectrum correspond to asymmetric and symmetric stretching vibrations of  $\text{-COO}^-$ . The band at  $1580\text{ cm}^{-1}$  is due to the azomethine bond of the Schiff base precursor.

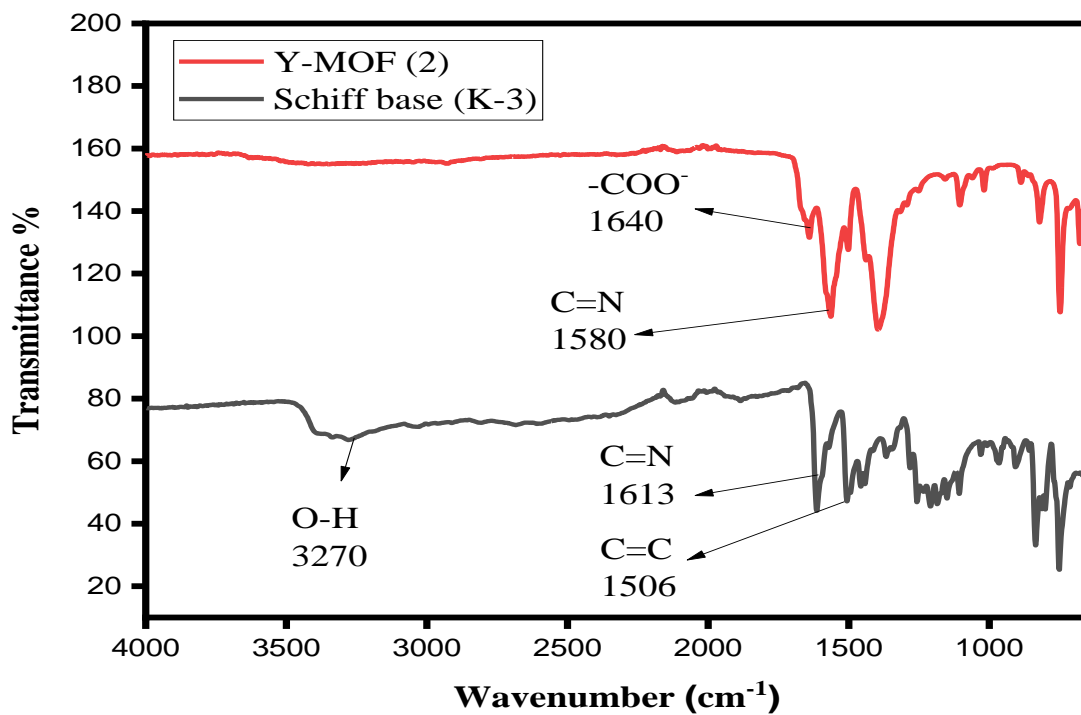


*Figure 20: FT-IR of Y-MOF (2)/ Schiff base (K-3)*

### 3.1.6.2 XRD of Y-MOF (2)

The figure 21 below depicts the XRD pattern of Y-MOF (2). The emergence of the peak at 6.4 degree served as confirmation of the successful development of MOF.

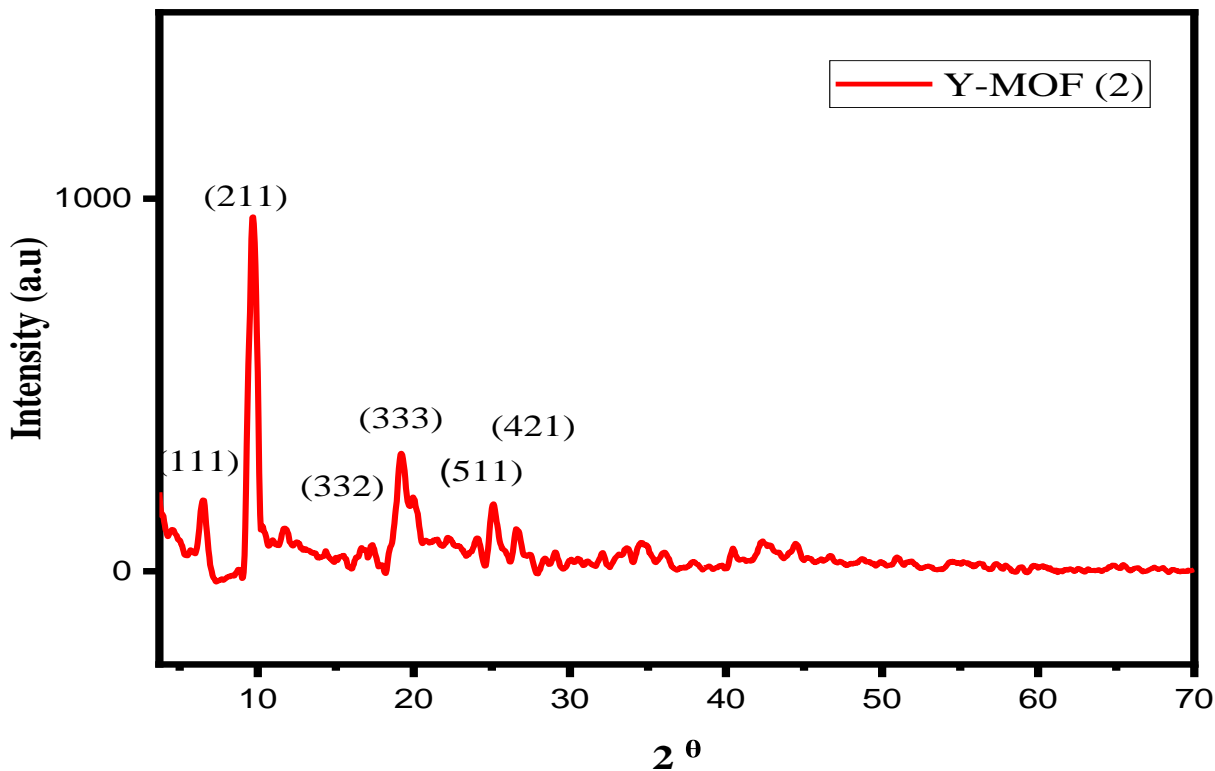


*Figure 21: XRD of Y-MOF (2)*

### 3.1.6.3 SEM of Y-MOF (2)

The SEM images at different resolutions of Y-MOF (2) are shown in figure 22. It can be seen from the SEM images that there are two distinctive morphologies present in the Y-MOF (1) which are nanoclusters and nanorods. The presence of nanorods depicts that building blocks of MOF are assembled to produce these elongated structures in a particular crystallographic direction. The nanoclusters could be formed due to the clustering of MOF particles.

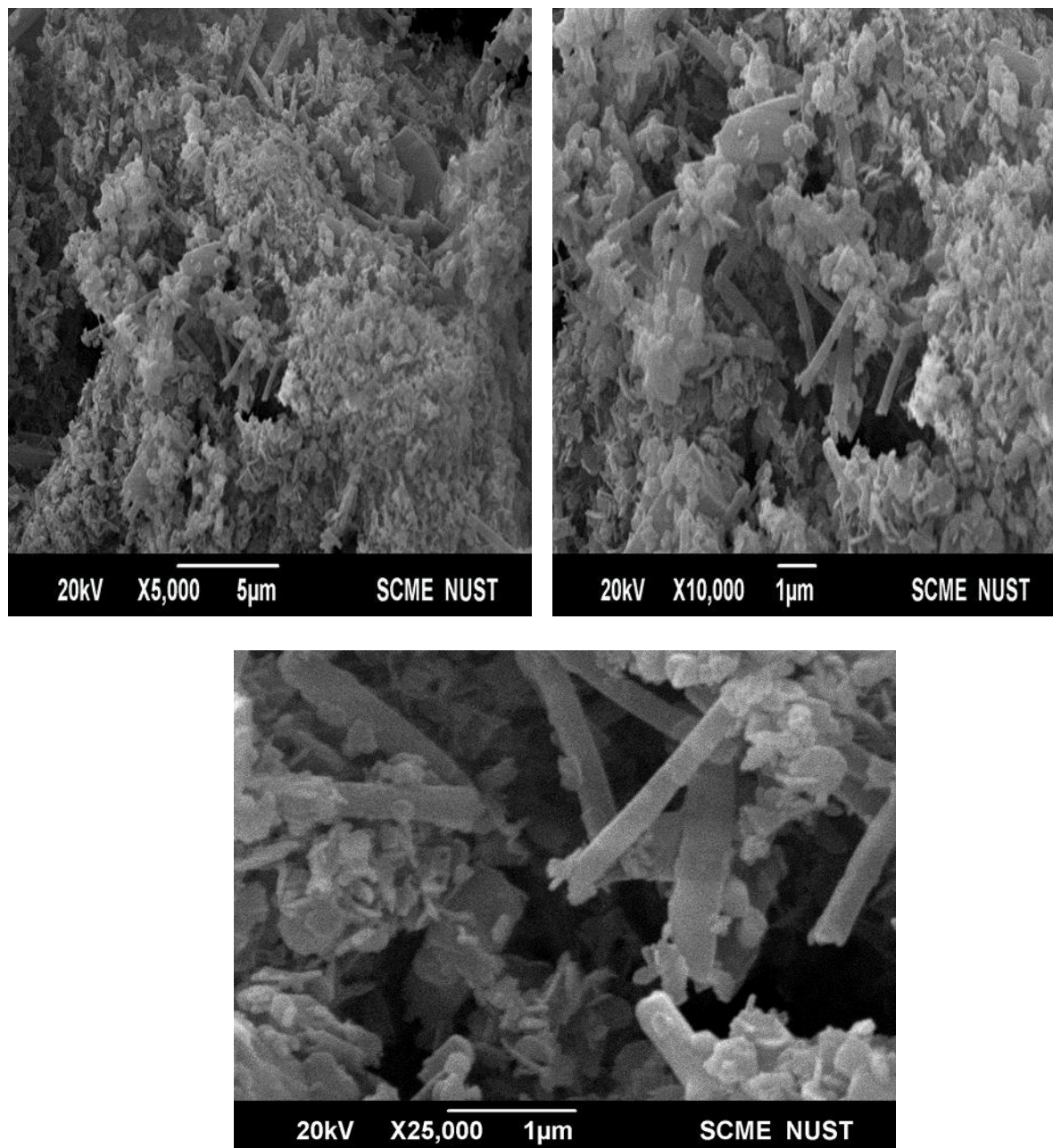


*Figure 22: SEM Images of Y-MOF (2) at Different Resolution*

### **3.1.7 EDX of Y-MOF (2)**

The chemical content of Y-MOF (2) was assessed using an Energy Dispersive X-ray Spectroscopy (EDX). This analysis visibly demonstrated the identification of prominent peaks with weight percentages of Y (27.7), C (46.3), and O (21.8) elements. And the spectrum in figure 23 does not contain any extra contaminants.

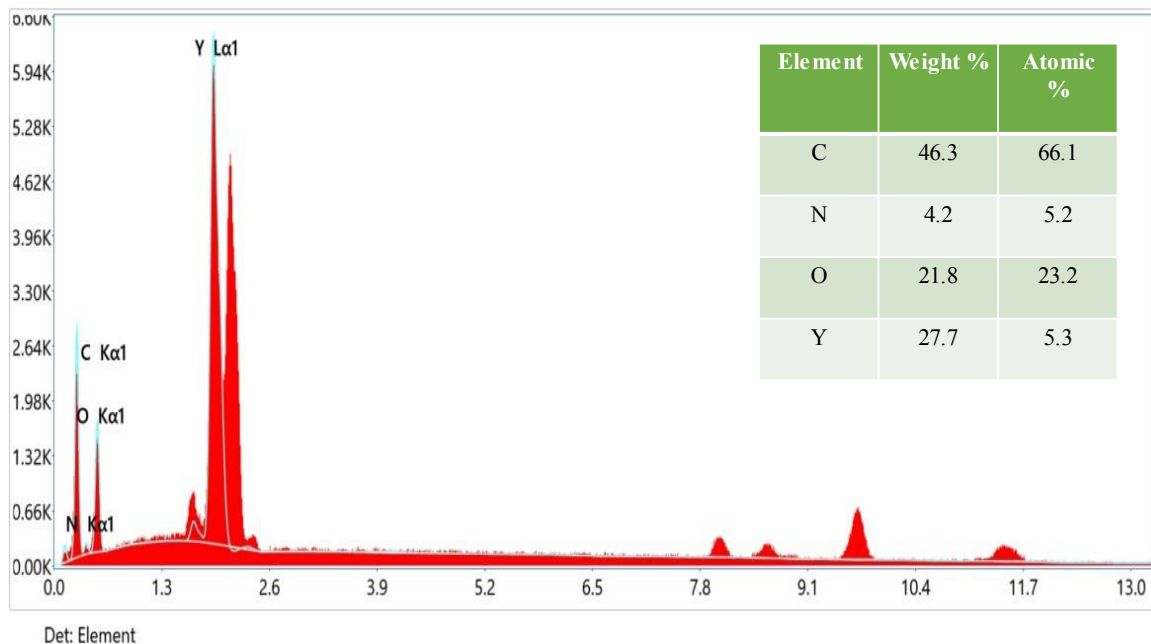


*Figure 23: EDX of Y-MOF (2)*

## 3.2 Electrocatalytic Water Splitting

### 3.2.1 Linear Sweep Voltammetry of Synthesized MOFs

Following a successful synthesis, steady-state electrochemical measurements were conducted on all the thin films. By investigating water oxidation voltametric curves in the potential range of 1.0-2.0 vs. RHE in 1M KOH, the catalytic responses were captured for the samples as prepared.

All the MOFs that had been synthesized had their voltages measured using linear sweep voltammetry. Y-MOF (1) demonstrated the current density of almost 180 mA/cm<sup>2</sup> and the lowest over potential of 280 mV, and Zn MOF showed current density about 230 mA/cm<sup>2</sup> and overpotential about 340 mV at 10 mA/cm<sup>2</sup>.

This is because the appropriate nano crystal structure, as shown in SEM images and XRD graph, was produced.

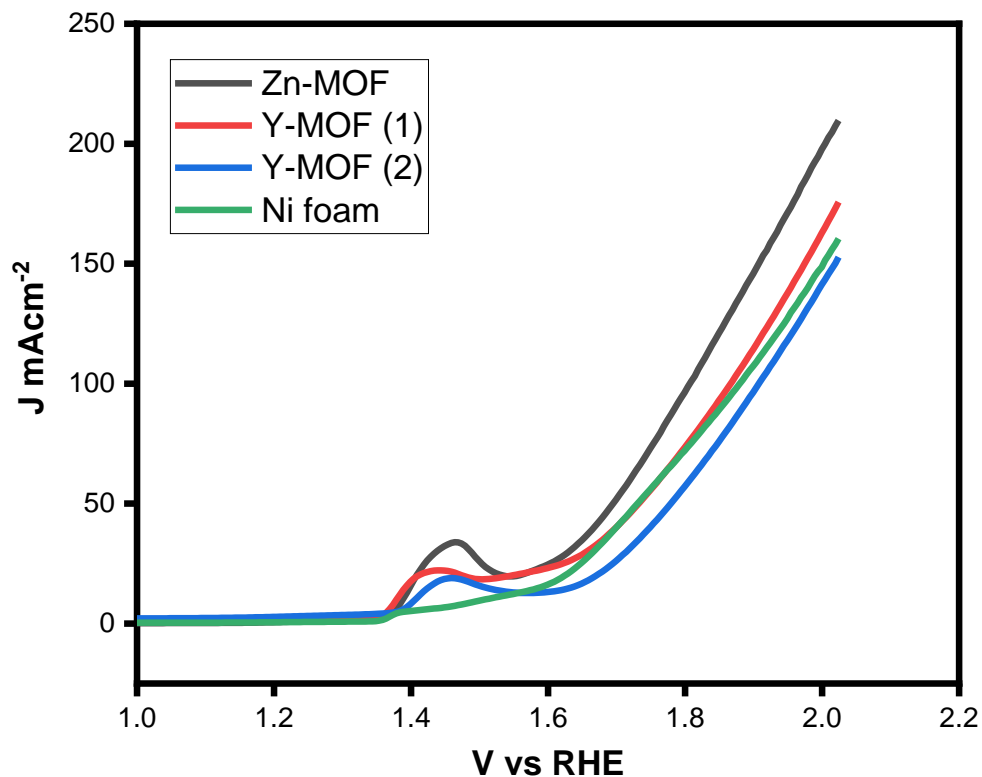


*Figure 24: Polarization Curves of all MOFs and Bare Ni-foam*

The overpotential at 10 mAcm<sup>-2</sup> of all the synthesized MOFs was shown in the table. The overpotential value of synthesized MOFs was calculated from reverse LSV curves, to rule out any uncertainties brought on by the pre-oxidation of nickel metal.

*Table 4: Overpotential Value of Synthesized MOFs*

Sample	Overpotential at 10 mAcm <sup>-2</sup> (mV)
Y-MOF (1)	280
Zn-MOF	340
Y-MOF (2)	410

### 3.2.2 Electrochemical impedance Spectroscopy

Electrochemical impedance spectroscopy was used to calculate the water oxidation kinetics of all the produced MOFs. To reduce the variation in solution resistance, fresh electrolyte was used for



all results. The resistance of the electrolyte is represented by the term "solution resistance," whereas the term "charge transfer resistance," or " $R_{ct}$ ," represents the interfacial resistance between the material and the electrolyte. The latter is the resistance that governs the charge transfer kinetics in the oxygen evolution reaction (OER). Faster charge transfer is correlated with lower  $R_{ct}$ <sup>61</sup>.

The trial-and-error method was used to set up a circuit for modeling the EIS data. The Nyquist graphs of each catalyst are shown in Figure 25. The circuit contained  $Y_0$ , and two resistors as shown in the figure 26.

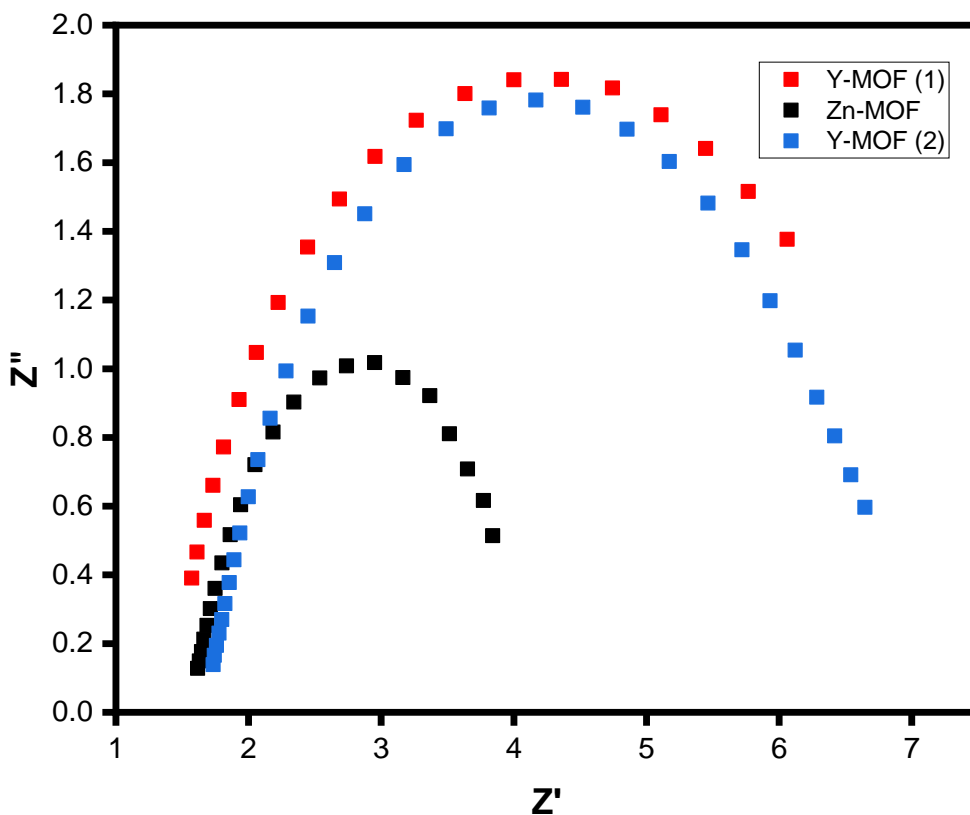


*Figure 25: EIS of Synthesized MOFs*

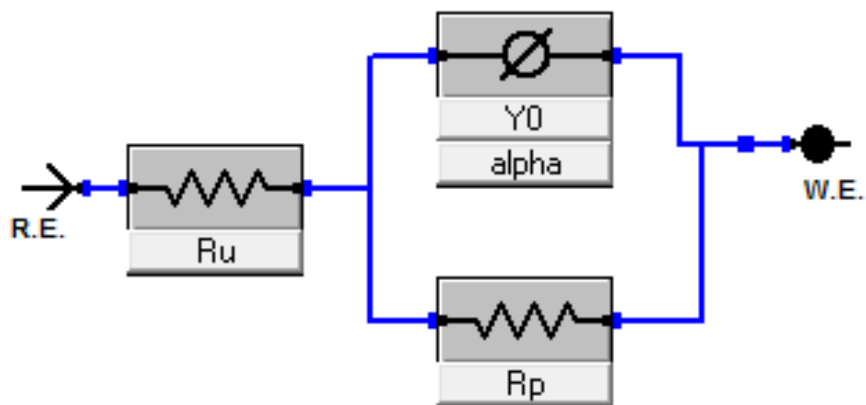


Figure 26: Fitted circuit.

The values of charge transfer resistance were given in the table below.

Table 5: Value of  $R_{ct}$  of all MOFs

MOF	$R_{ct}$ (ohm)
Zn- MOF	2.419
Y-MOF (1)	5.12
Y-MOF (2)	5.044

### 3.2.3 Chronoamperometry

Long-term stability of the catalyst is crucial for its commercialization and industrial use. Numerous techniques are used to examine the durability of materials. They are commonly assessed using chronopotentiometry, chronoamperometric, and repetitive linear sweep voltammetry scans at various voltage and current levels.

Chronopotentiometry (CP) and chronoamperometry (CA) are two studies in which the potential or current are fixed and the subsequent current or potential at the working electrode is measured<sup>62</sup>.

The as synthesized MOFs exhibited sustained OER potential values at constant current densities of  $50 \text{ mAcm}^{-2}$ . There are two main causes for the 40 mV, 60 mV and 70 mV voltage increase that were observed for Y-MOF (1), Y-MOF (2) and Zn-MOF respectively. The first possibility is that the electro catalyst may be removed from the electrode surface because of the production of  $\text{O}_2$  gas. Second, less efficient interaction between the catalyst and the electrolyte results from the production of  $\text{O}_2$  bubbles.

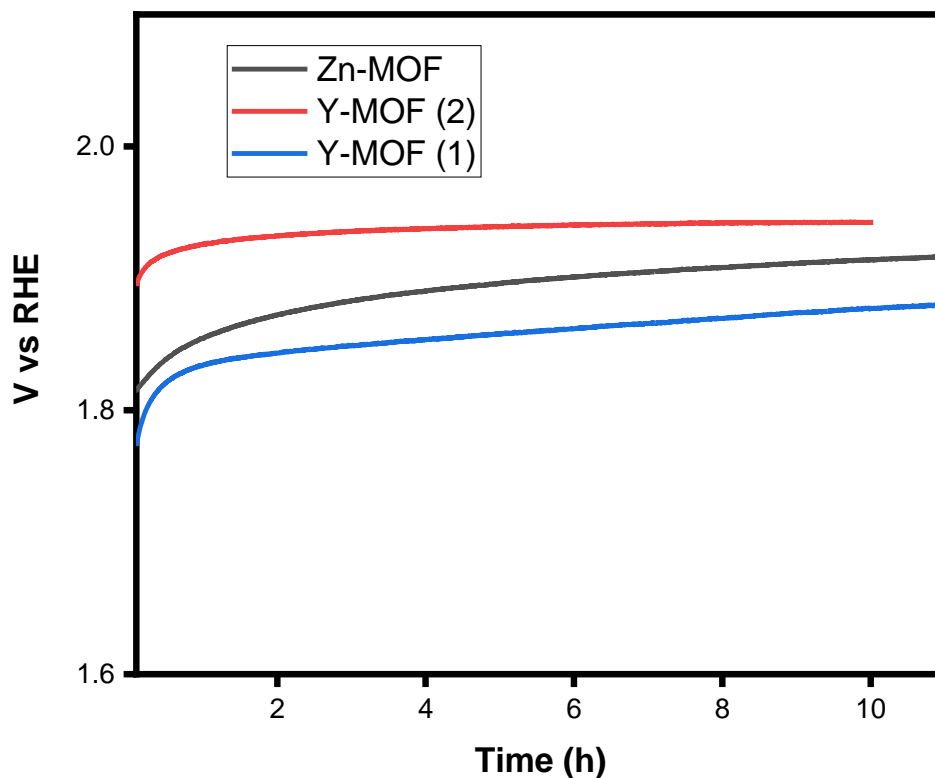


*Figure 27: CP plot for MOFs*

### 3.3 $\text{CO}_2$ Adsorption

The synthesized MOFs were also subjected to  $\text{CO}_2$  adsorption. The  $\text{CO}_2$  adsorption analysis was conducted at 310 K temperature and at 10 bar pressure. The adsorption isotherms for Y-MOF (2) and Zn-MOF are shown in Figure 28. It can be seen from the isotherms that the amount of adsorbed gas increases with increasing pressure. The maximum gas adsorbed at the MOF sites was  $0.08 \text{ mmol/g}$  and  $0.1 \text{ mmol/g}$  at 10 bar for Zn-MOF and Y-MOF (2) respectively.

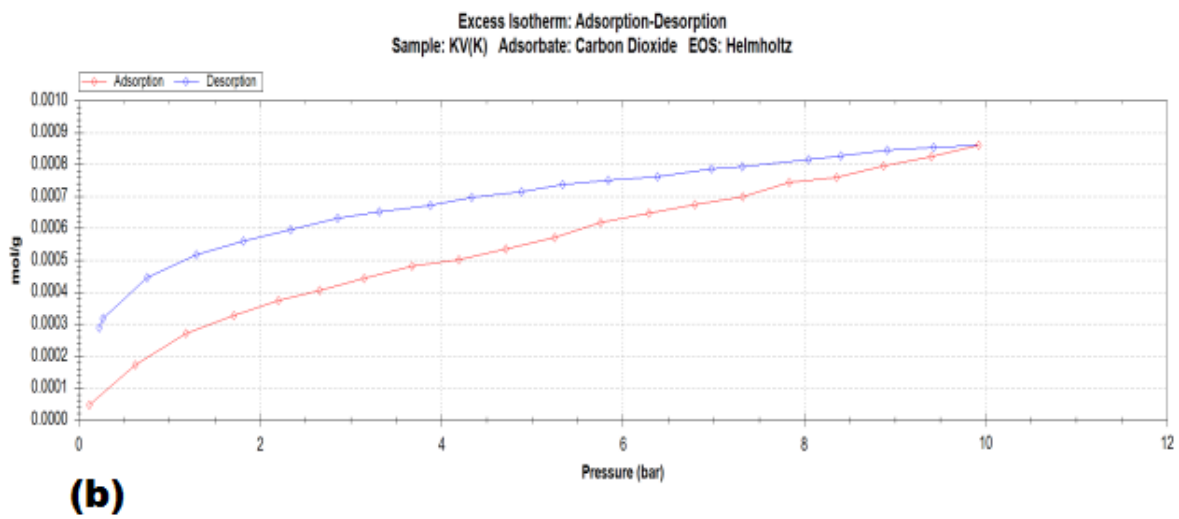
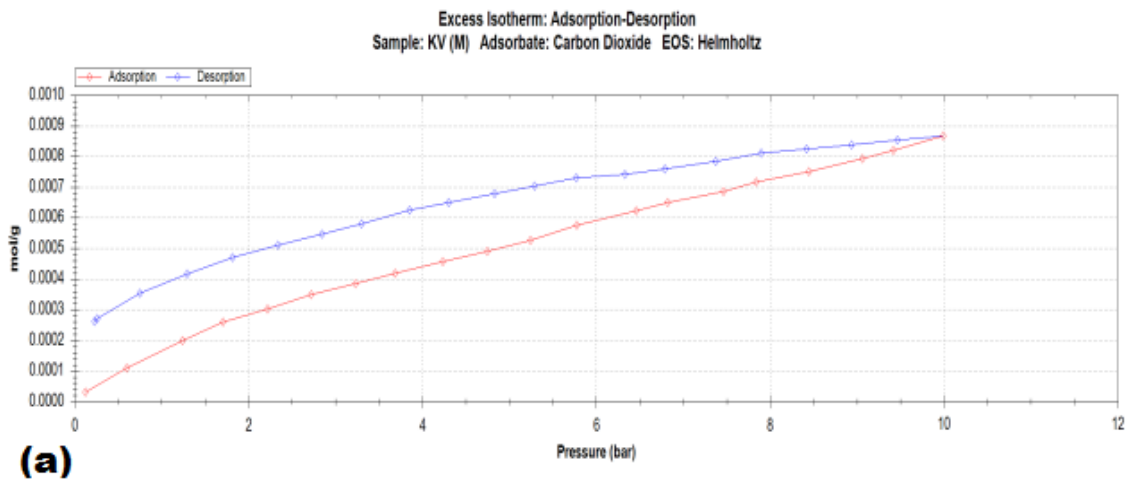


Figure 28: (a) Sorption Isotherm of Y-MOF (2) (b) Sorption Isotherm of Zn-MOF

## 4. Work Summary

*Table 6: Comparison of the results of OER of all MOFs*

Catalyst	Overpotential at 10 mAcm <sup>-1</sup>	Current density (mAcm <sup>-2</sup> )	R <sub>ct</sub> (ohm)
Zn-MOF	340	230	2.418
Y-MOF (1)	280	180	5.12
Y-MOF (2)	410	165	5.04

## 5. Conclusion

To sum things up, simple solvothermal synthesis was used to synthesize novel MOFs. The characterization of the synthesized MOFs included XRD, FT-IR, SEM, EDX, and TGA. The MOFs were tested for CO<sub>2</sub> adsorption and electrochemical water splitting. Zn-MOF demonstrated overpotential of 340 mV with current density of 230 mA/cm<sup>2</sup>, Y-MOF (1) demonstrated lowest overpotential of 280 mV with current density of 180 mA/cm<sup>2</sup>, and Y-MOF (2) shown highest overpotential of 420 mV. The Zn-MOF demonstrated the lowest charge transfer resistance, which was roughly 2.418 ohm. The produced MOFs were also chronopotentiometrically tested to ensure the stability of catalysts. They exhibited good stability for a period of ten hours. Y-MOF (2) exhibited moderate gas adsorption capacity.

## References:

- (1) Metal-Organic Frameworks History and Structural Features. In *Metal-Organic Framework Membranes for Molecular Gas Separations*; Series on Chemical Engineering; WORLD SCIENTIFIC (EUROPE), 2018; Vol. Volume 6, pp 1–29. [https://doi.org/doi:10.1142/9781786346735\\_0001](https://doi.org/doi:10.1142/9781786346735_0001).
- (2) Safaei, M.; Foroughi, M. M.; Ebrahimpoor, N.; Jahani, S.; Omid, A.; Khatami, M. A Review on Metal-Organic Frameworks: Synthesis and Applications. *TrAC Trends in Analytical Chemistry* **2019**, *118*, 401–425. <https://doi.org/10.1016/j.trac.2019.06.007>.
- (3) Butova, V.; Soldatov, M.; Guda, A.; Lomachenko, K.; Lamberti, C. Metal-Organic Frameworks: Structure, Properties, Methods of Synthesis, and Characterization. *Russian Chemical Reviews* **2016**, *85*, 280–307. <https://doi.org/10.1070/RCR4554>.
- (4) Rowsell, J. L. C.; Yaghi, O. M. Metal–Organic Frameworks: A New Class of Porous Materials. *Microporous and Mesoporous Materials* **2004**, *73* (1), 3–14. <https://doi.org/https://doi.org/10.1016/j.micromeso.2004.03.034>.
- (5) Metal-Organic Frameworks History and Structural Features. In *Metal-Organic Framework Membranes for Molecular Gas Separations*; Series on Chemical Engineering; WORLD SCIENTIFIC (EUROPE), 2018; Vol. Volume 6, pp 1–29. [https://doi.org/doi:10.1142/9781786346735\\_0001](https://doi.org/doi:10.1142/9781786346735_0001).
- (6) Janiak, C. Engineering Coordination Polymers towards Applications. *Dalton Transactions* **2003**, No. 14, 2781–2804. <https://doi.org/10.1039/B305705B>.
- (7) James, S. L. Metal-Organic Frameworks. *Chem Soc Rev* **2003**, *32* (5), 276–288. <https://doi.org/10.1039/B200393G>.
- (8) Raptopoulou, C. P. Metal-Organic Frameworks: Synthetic Methods and Potential Applications. *Materials* **2021**, *14*.

- (9) Stock, N.; Biswas, S. Synthesis of Metal-Organic Frameworks (MOFs): Routes to Various MOF Topologies, Morphologies, and Composites. *Chem Rev* **2012**, *112* (2), 933–969. <https://doi.org/10.1021/cr200304e>.
- (10) Jhung, S.-H.; Lee, J.-H.; Chang, J.-S. Microwave Synthesis of a Nanoporous Hybrid Material, Chromium Trimesate. *Bull Korean Chem Soc* **2005**, *26* (6), 880–881.
- (11) Lu, C.-M.; Liu, J.; Xiao, K.; Harris, A. T. Microwave Enhanced Synthesis of MOF-5 and Its CO<sub>2</sub> Capture Ability at Moderate Temperatures across Multiple Capture and Release Cycles. *Chemical Engineering Journal* **2010**, *156* (2), 465–470. <https://doi.org/https://doi.org/10.1016/j.cej.2009.10.067>.
- (12) Wu, X.; Bao, Z.; Yuan, B.; Wang, J.; Sun, Y.; Luo, H.; Deng, S. Microwave Synthesis and Characterization of MOF-74 (M = Ni, Mg) for Gas Separation. *Microporous and Mesoporous Materials* **2013**, *180*, 114–122. <https://doi.org/10.1016/J.MICROMESO.2013.06.023>.
- (13) Taddei, M.; Steitz, D. A.; van Bokhoven, J. A.; Ranocchiari, M. Continuous-Flow Microwave Synthesis of Metal–Organic Frameworks: A Highly Efficient Method for Large-Scale Production. *Chemistry – A European Journal* **2016**, *22* (10), 3245–3249. <https://doi.org/https://doi.org/10.1002/chem.201505139>.
- (14) Do, J.-L.; Friščić, T. Mechanochemistry: A Force of Synthesis. *ACS Cent Sci* **2017**, *3* (1), 13–19. <https://doi.org/10.1021/acscentsci.6b00277>.
- (15) Klimakow, M.; Klobes, P.; Thünemann, A. F.; Rademann, K.; Emmerling, F. Mechanochemical Synthesis of Metal–Organic Frameworks: A Fast and Facile Approach toward Quantitative Yields and High Specific Surface Areas. *Chemistry of Materials* **2010**, *22* (18), 5216–5221. <https://doi.org/10.1021/cm1012119>.
- (16) Lv, D.; Chen, Y.; Li, Y.; Shi, R.; Wu, H.; Sun, X.; Xiao, J.; Xi, H.; Xia, Q.; Li, Z. Efficient Mechanochemical Synthesis of MOF-5 for Linear Alkanes Adsorption. *J Chem Eng Data* **2017**, *62* (7), 2030–2036. <https://doi.org/10.1021/acs.jced.7b00049>.

- (17) Beamish-Cook, J.; Shankland, K.; Murray, C. A.; Vaquero, P. Insights into the Mechanochemical Synthesis of MOF-74. *Cryst Growth Des* **2021**, *21* (5), 3047–3055. <https://doi.org/10.1021/acs.cgd.1c00213>.
- (18) M. V., V.; Nageswaran, G. Review—Direct Electrochemical Synthesis of Metal Organic Frameworks. *J Electrochem Soc* **2020**, *167* (15), 155527. <https://doi.org/10.1149/1945-7111/abc6c6>.
- (19) Ghoorchian, A.; Afkhami, A.; Madrakian, T.; Ahmadi, M. Chapter 9 - Electrochemical Synthesis of MOFs. In *Metal-Organic Frameworks for Biomedical Applications*; Mozafari, M., Ed.; Woodhead Publishing, 2020; pp 177–195. <https://doi.org/https://doi.org/10.1016/B978-0-12-816984-1.00011-1>.
- (20) Wei, J.-Z.; Gong, F.-X.; Sun, X.-J.; Li, Y.; Zhang, T.; Zhao, X.-J.; Zhang, F.-M. Rapid and Low-Cost Electrochemical Synthesis of UiO-66-NH<sub>2</sub> with Enhanced Fluorescence Detection Performance. *Inorg Chem* **2019**, *58* (10), 6742–6747. <https://doi.org/10.1021/acs.inorgchem.9b00157>.
- (21) Martinez Joaristi, A.; Juan-Alcañiz, J.; Serra-Crespo, P.; Kapteijn, F.; Gascon, J. Electrochemical Synthesis of Some Archetypical Zn<sup>2+</sup>, Cu<sup>2+</sup>, and Al<sup>3+</sup> Metal Organic Frameworks. *Cryst Growth Des* **2012**, *12* (7), 3489–3498. <https://doi.org/10.1021/cg300552w>.
- (22) Cao, W.; Liu, Y.; Xu, F.; Li, J.; Li, D.; Du, G.; Chen, N. In Situ Electrochemical Synthesis of Rod-Like Ni-MOFs as Battery-Type Electrode for High Performance Hybrid Supercapacitor. *J Electrochem Soc* **2020**, *167* (5), 050503. <https://doi.org/10.1149/2.0072005JES>.
- (23) van Assche, T. R. C.; Desmet, G.; Ameloot, R.; de Vos, D. E.; Terryn, H.; Denayer, J. F. M. Electrochemical Synthesis of Thin HKUST-1 Layers on Copper Mesh. *Microporous and Mesoporous Materials* **2012**, *158*, 209–213. <https://doi.org/https://doi.org/10.1016/j.micromeso.2012.03.029>.



- (24) Vehrenberg, J.; Veps€ Al€ Ainen, M.; Macedo, D. S.; Rubio-Martinez, M.; Webster, N. A. S.; Wessling, M. Steady-State Electrochemical Synthesis of HKUST-1 with Polarity Reversal. **2020**. <https://doi.org/10.1016/j.micromeso.2020.110218>.
- (25) Qiao, S. Z.; Liu, J.; Max Lu, G. Q. Synthetic Chemistry of Nanomaterials. *Modern Inorganic Synthetic Chemistry: Second Edition* **2017**, 613–640. <https://doi.org/10.1016/B978-0-444-63591-4.00021-5>.
- (26) G. Carson, C.; J. Brown, A.; S. Sholl, D.; Nair, S. Sonochemical Synthesis and Characterization of Submicrometer Crystals of the Metal–Organic Framework Cu[(Hfipbb)(H2hfipbb)0.5]. *Crystal Growth & Design* **2011**, *11* (10), 4505–4510. <https://doi.org/10.1021/cg200728b>.
- (27) Yu, K.; Lee, Y. R.; Seo, J. Y.; Baek, K. Y.; Chung, Y. M.; Ahn, W. S. Sonochemical Synthesis of Zr-Based Porphyrinic MOF-525 and MOF-545: Enhancement in Catalytic and Adsorption Properties. *Microporous and Mesoporous Materials* **2021**, *316*, 110985. <https://doi.org/10.1016/J.MICROMESO.2021.110985>.
- (28) Jung, D. W.; Yang, D. A.; Kim, J.; Kim, J.; Ahn, W. S. Facile Synthesis of MOF-177 by a Sonochemical Method Using 1-Methyl-2-Pyrrolidinone as a Solvent. *Dalton Transactions* **2010**, *39* (11), 2883–2887. <https://doi.org/10.1039/B925088C>.
- (29) Israr, F.; Chun, D.; Kim, Y.; Kim, D. K. High Yield Synthesis of Ni-BTC Metal–Organic Framework with Ultrasonic Irradiation: Role of Polar Aprotic DMF Solvent. *Ultrason Sonochem* **2016**, *31*, 93–101. <https://doi.org/https://doi.org/10.1016/j.ultsonch.2015.12.007>.
- (30) Kalaj, M.; Cohen, S. M. Postsynthetic Modification: An Enabling Technology for the Advancement of Metal-Organic Frameworks. *ACS Cent Sci* **2020**, *6* (7), 1046–1057. [https://doi.org/10.1021/ACSCENTSCI.0C00690/ASSET/IMAGES/LARGE/OC0C00690\\_0007.JPEG](https://doi.org/10.1021/ACSCENTSCI.0C00690/ASSET/IMAGES/LARGE/OC0C00690_0007.JPEG).
- (31) Mandal, S.; Natarajan, S.; Mani, P.; Pankajakshan, A. Post-Synthetic Modification of Metal–Organic Frameworks Toward Applications. *Adv Funct Mater* **2021**, *31* (4), 2006291. <https://doi.org/https://doi.org/10.1002/adfm.202006291>.

- (32) Pettinari, C.; Marchetti, F.; Mosca, N.; Tosi, G.; Drozdov, A. Application of Metal – Organic Frameworks. *Polym Int* **2017**, *66* (6), 731–744. <https://doi.org/https://doi.org/10.1002/pi.5315>.
- (33) Kuppler, R. J.; Timmons, D. J.; Fang, Q.-R.; Li, J.-R.; Makal, T. A.; Young, M. D.; Yuan, D.; Zhao, D.; Zhuang, W.; Zhou, H.-C. Potential Applications of Metal-Organic Frameworks. *Coord Chem Rev* **2009**, *253* (23), 3042–3066. <https://doi.org/https://doi.org/10.1016/j.ccr.2009.05.019>.
- (34) Keskin, S.; Kızılel, S. Biomedical Applications of Metal Organic Frameworks. *Industrial & Engineering Chemistry Research* **2011**, *50* (4), 1799–1812. <https://doi.org/10.1021/ie101312k>.
- (35) Filippousi, M.; Turner, S.; Leus, K.; Siafaka, P. I.; Tseligka, E. D.; Vandichel, M.; Nanaki, S. G.; Vizirianakis, I. S.; Bikiaris, D. N.; van der Voort, P.; van Tendeloo, G. Biocompatible Zr-Based Nanoscale MOFs Coated with Modified Poly( $\epsilon$ -Caprolactone) as Anticancer Drug Carriers. *Int J Pharm* **2016**, *509* (1), 208–218. <https://doi.org/https://doi.org/10.1016/j.ijpharm.2016.05.048>.
- (36) Zhang, L.; Chen, Y.; Shi, R.; Kang, T.; Pang, G.; Wang, B.; Zhao, Y.; Zeng, X.; Zou, C.; Wu, P.; Li, J. Synthesis of Hollow Nanocages MOF-5 as Drug Delivery Vehicle to Solve the Load-Bearing Problem of Insoluble Antitumor Drug Oleanolic Acid (OA). *Inorg Chem Commun* **2018**, *96*, 20–23. <https://doi.org/https://doi.org/10.1016/j.inoche.2018.07.029>.
- (37) Xie, Y.; Liu, X.; Ma, X.; Duan, Y.; Yao, Y.; Cai, Q. Small Titanium-Based MOFs Prepared with the Introduction of Tetraethyl Orthosilicate and Their Potential for Use in Drug Delivery. *ACS Applied Materials & Interfaces* **2018**, *10* (16), 13325–13332. <https://doi.org/10.1021/acsami.8b01175>.
- (38) Lin, R.-B.; Xiang, S.; Xing, H.; Zhou, W.; Chen, B. Exploration of Porous Metal–Organic Frameworks for Gas Separation and Purification. *Coord Chem Rev* **2019**, *378*, 87–103. <https://doi.org/https://doi.org/10.1016/j.ccr.2017.09.027>.

- (39) Aykac Ozen, H.; Ozturk, B. Gas Separation Characteristic of Mixed Matrix Membrane Prepared by MOF-5 Including Different Metals. *Sep Purif Technol* **2019**, *211*, 514–521. <https://doi.org/https://doi.org/10.1016/j.seppur.2018.09.052>.
- (40) Huang, K.; Liu, S.; Li, Q.; Jin, W. Preparation of Novel Metal-Carboxylate System MOF Membrane for Gas Separation. *Sep Purif Technol* **2013**, *119*, 94–101. <https://doi.org/10.1016/J.SEPPUR.2013.09.008>.
- (41) Zhao, Z.; Ma, X.; Kasik, A.; Li, Z.; S. Lin, Y. Gas Separation Properties of Metal Organic Framework (MOF-5) Membranes. *Industrial & Engineering Chemistry Research* **2012**, *52* (3), 1102–1108. <https://doi.org/10.1021/ie202777q>.
- (42) Li, Y.-Z.; Wang, G.-D.; Yang, H.-Y.; Hou, L.; Wang, Y.-Y.; Zhu, Z. Novel Cage-like MOF for Gas Separation, CO<sub>2</sub> Conversion and Selective Adsorption of an Organic Dye. *Inorg Chem Front* **2020**, *7* (3), 746–755. <https://doi.org/10.1039/C9QI01262A>.
- (43) Li, D.; Xu, H.-Q.; Jiao, L.; Jiang, H.-L. Metal-Organic Frameworks for Catalysis: State of the Art, Challenges, and Opportunities. *EnergyChem* **2019**, *1* (1), 100005. <https://doi.org/https://doi.org/10.1016/j.enchem.2019.100005>.
- (44) Llabrés i Xamena, F. X.; Abad, A.; Corma, A.; Garcia, H. MOFs as Catalysts: Activity, Reusability and Shape-Selectivity of a Pd-Containing MOF. *J Catal* **2007**, *250* (2), 294–298. <https://doi.org/10.1016/J.JCAT.2007.06.004>.
- (45) Hu, R.; Zhang, X.; Chi, K.-N.; Yang, T.; Yang, Y.-H. Bifunctional MOFs-Based Ratiometric Electrochemical Sensor for Multiplex Heavy Metal Ions. *ACS Applied Materials & Interfaces* **2020**, *12* (27), 30770–30778. <https://doi.org/10.1021/acsami.0c06291>.
- (46) Hu, R.; Zhang, X.; Chi, K.-N.; Yang, T.; Yang, Y.-H. Bifunctional MOFs-Based Ratiometric Electrochemical Sensor for Multiplex Heavy Metal Ions. *ACS Applied Materials & Interfaces* **2020**, *12* (27), 30770–30778. <https://doi.org/10.1021/acsami.0c06291>.
- (47) Ma, D.; Li, B.; Zhou, X.; Zhou, Q.; Liu, K.; Zeng, G.; Li, G.; Shi, Z.; Feng, S. A Dual Functional MOF as a Luminescent Sensor for Quantitatively Detecting the Concentration

- of Nitrobenzene and Temperature. *Chemical Communications* **2013**, 49 (79), 8964–8966. <https://doi.org/10.1039/C3CC44546A>.
- (48) Li, H.; Wang, K.; Sun, Y.; Lollar, C. T.; Li, J.; Zhou, H. C. Recent Advances in Gas Storage and Separation Using Metal–Organic Frameworks. *Materials Today* **2018**, 21 (2), 108–121. <https://doi.org/10.1016/J.MATTOD.2017.07.006>.
- (49) Zhang, B.; Zheng, Y.; Ma, T.; Yang, C.; Peng, Y.; Zhou, Z.; Zhou, M.; Li, S.; Wang, Y.; Cheng, C. Designing MOF Nanoarchitectures for Electrochemical Water Splitting. *Advanced Materials* **2021**, 33 (17), 2006042. <https://doi.org/https://doi.org/10.1002/adma.202006042>.
- (50) Dutta, R.; Shrivastav, R.; Srivastava, M.; Verma, A.; Saxena, S.; Biswas, N. K.; Satsangi, V. R.; Dass, S. MOFs in Photoelectrochemical Water Splitting: New Horizons and Challenges. *Int J Hydrogen Energy* **2022**, 47 (8), 5192–5210. <https://doi.org/10.1016/J.IJHYDENE.2021.11.185>.
- (51) Zhou, X.; Shao, L.; Jin, Z.; Liu, J. B.; Dai, H.; Fang, J. X. Synthesis and Antitumor Activity Evaluation of Some Schiff Bases Derived from 2-Aminothiazole Derivatives. *Heteroatom Chemistry* **2007**, 18 (1), 55–59. <https://doi.org/10.1002/HC.20256>.
- (52) Yaqoob, L.; Noor, T.; Iqbal, N.; Nasir, H.; Zaman, N.; Talha, K. Electrochemical Synergies of Fe–Ni Bimetallic MOF CNTs Catalyst for OER in Water Splitting. *J Alloys Compd* **2021**, 850, 156583. <https://doi.org/10.1016/J.JALLCOM.2020.156583>.
- (53) Bunaciu, A. A.; Udriștioiu, E. gabriela; Aboul-Enein, H. Y. X-Ray Diffraction: Instrumentation and Applications. *Crit Rev Anal Chem* **2015**, 45 (4), 289–299. <https://doi.org/10.1080/10408347.2014.949616>.
- (54) Silva, T. A.; Stefano, J. S.; Janegitz, B. C. Sensing Materials: Nanomaterials. *Encyclopedia of Sensors and Biosensors* **2023**, 212–230. <https://doi.org/10.1016/B978-0-12-822548-6.00023-6>.
- (55) Singh, A. K. Experimental Methodologies for the Characterization of Nanoparticles. *Engineered Nanoparticles* **2016**, 125–170. <https://doi.org/10.1016/B978-0-12-801406-6.00004-2>.

- (56) Colpan, C. O.; Nalbant, Y.; Ercelik, M. 4.28 Fundamentals of Fuel Cell Technologies. *Comprehensive Energy Systems* **2018**, 4–5, 1107–1130. <https://doi.org/10.1016/B978-0-12-809597-3.00446-6>.
- (57) Song, K. Interphase Characterization in Rubber Nanocomposites. *Progress in Rubber Nanocomposites* **2017**, 115–152. <https://doi.org/10.1016/B978-0-08-100409-8.00004-8>.
- (58) El-Sonbati, A. Z.; Mahmoud, W. H.; Mohamed, G. G.; Diab, M. A.; Morgan, S. M.; Abbas, S. Y. Synthesis, Characterization of Schiff Base Metal Complexes and Their Biological Investigation. *Appl Organomet Chem* **2019**, 33 (9). <https://doi.org/10.1002/AOC.5048>.
- (59) Lou, X.; Hu, H.; Li, C.; Hu, X.; Li, T.; Shen, M.; Chen, Q.; Hu, B. Capacity Control of Ferric Coordination Polymers by Zinc Nitrate for Lithium-Ion Batteries. *RSC Adv* **2016**, 6 (89), 86126–86130. <https://doi.org/10.1039/C6RA17608A>.
- (60) Akbarzadeh, F.; Motaghi, M.; Chauhan, N. P. S.; Sargazi, G. A Novel Synthesis of New Antibacterial Nanostructures Based on Zn-MOF Compound: Design, Characterization and a High Performance Application. *Heliyon* **2020**, 6 (1). <https://doi.org/10.1016/J.HELIYON.2020.E03231>.
- (61) Zhang, X.; Luo, J.; Wan, K.; Plessers, D.; Sels, B.; Song, J.; Chen, L.; Zhang, T.; Tang, P.; Morante, J. R.; Arbiol, J.; Fransaer, J. From Rational Design of a New Bimetallic MOF Family with Tunable Linkers to OER Catalysts. *J Mater Chem A Mater* **2019**, 7 (4), 1616–1628. <https://doi.org/10.1039/C8TA08508K>.
- (62) Leslie, N.; Mauzeroll, J. Spatially Resolved Electrochemical Measurements. *Reference Module in Chemistry, Molecular Sciences and Chemical Engineering* **2023**. <https://doi.org/10.1016/B978-0-323-85669-0.00004-0>.